Graphene-based Coatings for Heat Exchangers

Master Thesis

Marie Långberg

VT 2015

Supervisors:
Dr. Karin Persson, Senior Project Manager, SP
Professor Reine Wallenberg, LTH

Examiner:
Professor Sven Lidin, LTH

Acronyms

Abbreviation	Full name
GO	Graphene oxide
GO_W	Graphene Oxide, water dispersed
AGO	Ammonia functionalized Graphene Oxide, water dispersed
PAni	Polyaniline
PAni AGO	Polyaniline grafted Ammonia functionalized Graphene Oxide
SEM	Scanning Electron Microscope
TEM	Transmission Electron Microscope
AFM	Atomic Force Microscope
NEMD	Non-Equilibrium Molecular dynamics
RGO	Reduced graphene oxide
GRM	Graphene related materials
NMP	N-Methyl 2-pyrolidone

Abstract

This master thesis is a part of a larger interwork between SP, KTH and Alfa Laval funded by the SIO graphene programme, which end goal is to formulate an anti-corrosion coating based on graphene or graphene related materials (GRMs). The investigation is partly based on an article "*Novel anticorrosion coatings prepared from polyaniline/graphene composites*" from 2012 by Chang et al in combination of knowledge acquired during a previous EU project, www.steelcoatproject.com concerning polyaniline for anti-corrosion coatings. The purpose of this master thesis is to optimize the synthesis of the, PAni, and GRM nanocomposite.

Two different primary products of graphene oxides were investigated; water dispersed graphene oxide monolayer, GO_W and water dispersed ammonia functionalized graphene oxide, AGO. These investigations were made to be able to confirm the presence of single sheets, the hybridizations of carbon and particle appearance and sheet size.

A polyaniline/AGO nanocomposite made at SP before the initiation of this master thesis containing 20 wt% AGO was analyzed by Raman spectroscopy, SEM, TEM and AFM. The reaction at which the SP nanocomposite was made was reviewed to find improvements. Agglomeration occurs when AGO is added to the reaction mixture of aniline monomers and hydrochloric acid. Improvements were investigated by analyzing the pH during the synthesis and the usage of ultrasonication. The later tests were made with an AGO load of 1 wt% and was analyzed by SEM and Raman spectroscopy. The synthesis using an ultrasonication step showed the best dispersion according to the visual appearance and the intensity ratio between sp^2 and sp^3 bonds in the Raman spectra.

Conclusion of this work is that the GRM products contain single sheets of the size of 1-7 µm for GO_W and 4-10 µm for AGO, with a sp^3/sp^2 ratio of around 1. The PAni/AGO should be ultra-sonicated to obtain a well dispersed solution of AGO and aniline monomers before the synthesis is started by addition of the initiator.

List of Contents

Key persons and figure acknowledgement
Dr Jens Sommertune, helped with polymer expertise, he also demonstrated the original PAni synthesis and provided the first batch of PAni/GRM.
Dr Birgit Brandner preformed the Raman analysis and helped with the data analysis using the software program Origin.
Annika Dahlman provided the SEM micrograph in Figure 14.
Rodrigo Robinson provided the SEM micrographs in Figures 1, 23-26.
Professor Reine Wallenberg helped with the TEM micrographs in Figure 21.
Dr Viveca Wallqvist provided the AFM micrographs in Figure 15- 16 and 19-20.
Dr Olga Santos that performed the application tests of the binders.

1. Introduction

1.1 General Introduction

Plate heat exchangers have large industrial value because of their high capability to transfer and recover heat from one fluid with higher temperature to another with low temperature. Heat exchangers have thin walls with good heat conducting properties to separate them. Materials used for the walls are for example nickel alloys, titanium alloys and stainless steel depending on the application. [1] The stainless steel anti-corrosion property is due to an oxidized chromium film on the surface. However, after being exposed for conditions like saline environment the stainless steel can start to corrode despite its high resistance. [2] Therefore it is important to find a coating that can enhance the anti-corrosion properties of the stainless steel further and by that extended the lifetime of the heat exchanger.

The coating should be able to be permanently attached to the steel surface and still conduct the heat through the wall without any major reduction in the heat exchangers performance. One material that has excellent heat conduction properties is graphene. It has been reported that pristine graphene sheet has a thermal conductivity between 4840 – 5300 W/mK. [3] However, the graphene does not adhere to the steel surface by itself and therefore needs to be incorporated into binders. Additionally GRMs can be added to the binders to create a nanocomposite with desired properties like barrier, cohesion, adhesion to the substrate and anti-corrosion properties.

1.2 Project Background

This project is a part of a three part collaboration project between SP, KTH and Alfa Laval that together want to create novel corrosion protective coatings for plate heat exchangers. The end goal of the whole project is to formulate a graphene based anti-corrosion coating that retains the heat capacity of the heat exchangers which protects stainless steel from corrosion in saline conditions at 70-90^{o}C and should also be resistant for short cleaning periods of high and low pH. The project comprises two different paths that are investigated, one using polyaniline (PAni)/GRM nanocomposite and one using GO dispersions with well established commercial binders with excellent anti-corrosion properties.

The project is funded by Vinnova and investigates polyaniline/graphene composites inspired by the article "*Novel anticorrosion coatings prepared from polyaniline/graphene composites*" from 2012 by Chang et al and also on knowledge acquired during a previous EU project about environment friendly steel coatings for anticorrosion applications, where novel ideas of the corrosion inhibition mechanism of polyaniline was analyzed but for mild steel. More information of the EU project can be found at www.steelcoatproject.com.

1.3 Purpose

The end goal of the whole project is to formulate a graphene based nanocomposite that can protect stainless steel against corrosion.

The purpose of this master thesis is to optimize the PAni/GRM synthesis.

1.4 Limitation

This thesis will focus on the synthesis of polyaniline graphene oxide nanocomposite, without any subsequent reduction of the oxides. There will also be some initial investigations of three commercial water based binders, where Alfa laval studied the adhesion properties of these coatings.

The analyzing methods used are restricted to SEM, TEM, Nanosizer, Raman spectroscopy, AFM and TEM

2. Background

2.1 Stainless Steel and Corrosion

Stainless steel is more corrosion resistant than other steel alloys because of the chromium oxide/hydroxide that forms a passive film located on its surface. During production of steel the chromium located on the steel surface instantly reacts with oxygen and form Cr_2O_3. Chromium reacts to a larger extent with oxygen than the steel bulk metals such as iron and nickel because it has the highest affinity of the bulk metals in combination with oxygen. [4] The corrosion inhibition is improved by enrichment of chromium in the surface. The optimal level for corrosion protection is a content of 30 wt% because this is where the passivation of the stainless steel is the highest due to the chromium oxide film. Stainless steel needs at least 12 wt% to be able to be called stainless, but the oxide film can form at a level of 10 wt%. The level of chromium is restricted by the possibility of compromising some of the properties of steel such as alloy stability. Because of its resistance to corrosion, stainless steel has several fields of applications like medicine, food and technical industry. [2]

The microstructure of steel can be seen by using appropriate microscopes, like SEM, Figure 1. This technique makes it possible to reveal the steel structure with grains isolated by grain boundaries.

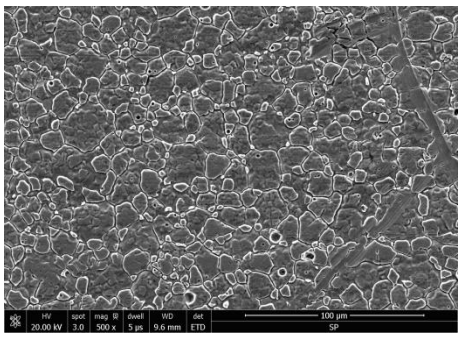

Figure 1: SEM micrographs of Stainless steel 316L the scale bar is 100 µm. SEM micrograph by R. Robinson.

Corrosion can occur because of environmental impacts despite a protecting film of chromium oxide. Environmental corrosion can for example be caused by salt, high and low pH, microorganisms or water alone. One of many definitions of corrosion, which is an umbrella term of many complex mechanisms, is according to Davis, J.R.: a systems reaction with its environment that impairs the properties that the system possesses. Corrosion occurs because of the natural tendency of a material to strive to the lowest energy state possible in its environment. A metal corrodes faster if it is subjected to a demanding environment with high water, oxygen and salt content. [5]

Iron is the most corrosive-prone substance in steel because when it reacts with oxygen it goes back to its original chemical form which is the same as in iron ore, $Fe_2O_3*H_2O$ [5]. Iron on the steel surface can in alkaline environments form an oxide film which can be seen in the white areas in the Pourbaix diagram in Figure 2. This oxide film has barrier properties which decreases the corrosion rate. [6, 7]

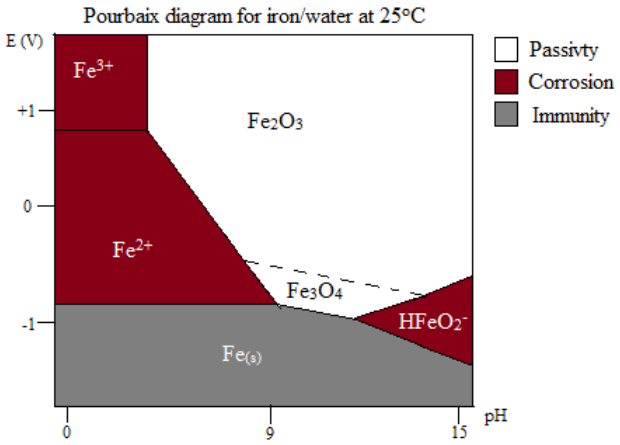

Figure 2: Pourbaix diagram for iron at 25°C, made after [7-9]

The application and thus the environmental condition the steel are exposed to affect the corrosion mechanism. For example, natural water has higher sodium chloride content than tap water which contributes to corrosion. [6, 7] When chlorides is involved the reaction mechanisms is, according to F.Y. Ma, [10]:

$$FeCl_2 + 2H_2O \rightarrow Fe(OH)_2 + 2HCl$$

The general reaction of corrosion from literature D. A. Bayliss and D. H. Deacon, [6]:

$$Anodic\ reaction: Fe \rightarrow Fe^{2+} + 2e^-$$

$$Cathodic\ reaction: \frac{1}{2}O_2 + H_2O + 2e^- \rightarrow 2OH^-$$

$$Total\ reaction: Fe + \frac{1}{2}O_2 + H_2O \rightarrow 2OH^- + Fe^{2+} \rightarrow$$

$$\rightarrow Fe(OH)_2 \xrightarrow{further\ oxidation} Fe_2O_3 * H_2O$$

Despite that Fe_2O_3 is passive the barrier properties of the substance are relatively poor compared to the stainless properties provided by chromiumoxide/hydroxide on the surface. To increase the lifetime of steels and other metals, corrosion can be inhibited by not only the design and choice of the metal alloy composition but also by coatings and inhibitors. Coatings can be made of noble metals that oxidize on the surface. The coatings can also be organic substances which can act as an isolating protection reduces the transport of ions and moisture to the surface of the metal substrate. Coatings can be doped with inhibitors and additives to increase the corrosion inhibition property. Inhibitors are surface adsorbed substances added to the corroding medium or in a coating to limit corrosion mechanism. [5]

There are many different kinds of stainless steels such as austenitic, ferric, duplex and martensitic steel where the main differences are the microstructure and the bulk composition. [11]

2.2 Graphene and Graphene Oxide

2.2.1 Graphene Introduction

Graphene is famous for its diversity of interesting properties like high electric and thermal conduction and therefore there have been a lot of investigations in different application fields, like in solar cells, touch screens, electrodes and transistors among others. [12, 13] Another example for the use of GRMs is in anti-corrosion coatings. Graphene can improve anti-corrosion protection because of its barrier properties for water and chloride ions in gaseous and in water applications. [14, 15]

Graphene is simply a single layer of the planar structure of graphite. It was first isolated in the beginning of the 21th century and since then the world of science exploded with investigations of possible application for this sp^2-hybridized carbon structure. The advantages with this one atom layer thick substance is for instance the high thermal conductivity, electrical conductivity, barrier property, lightweight and high strength among many others. The core of many of these properties is the regular honeycomb structure seen in Figure 3. [13]

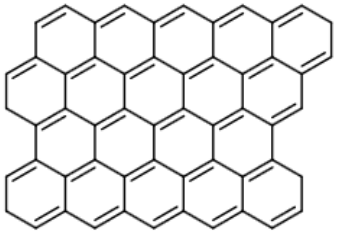

Figure 3: The structure of graphene. After Graphenea [16]

Production Processes of Graphene

Graphite contains several layers of graphene sheets and by exfoliations processes, graphene can be produced. Many processes are made in solutions. For example K. R. Paton et al, [17] has demonstrated scale able production methods in NMP, aqueous/surfactant solutions and that exfoliation occur when the local shear rate exceeds 10^4 s^{-1}. Graphene can also be grown by chemical vapor deposition where a silicon or copper substrate is used. [17, 18]

2.2.2 Graphene Oxide

Graphene is difficult to disperse in polar solvents, instead GO can be used because of the polar functional groups of oxygen makes the sheets more hydrophilic. The hydrophilic properties of the GO sheets make it possible to exfoliate them in many solvents and even water. [19] The oxidation procedure is often made by Hummers method, (Hummers method is shortly; graphite flakes mixed with sodium nitrate in sulfuric acid and then potassium permanganate is added as an oxidizing agent [20]). The oxidation increase the distance between the sheets. By dispersing the graphite oxide in a polar solvent the sheets can separate to single graphene oxide sheets. [19] Graphene oxide will for now on be abbreviated GO. A schematic of the structure of GO can be seen in Figure 4.

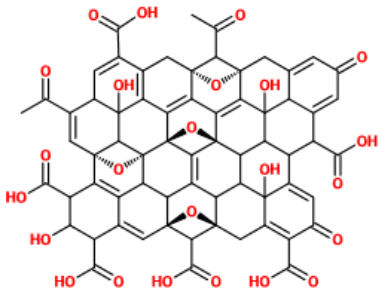

Figure 4: One possible structure of graphene oxide. After [18]

By oxidation of the graphite and thereby the graphene sheets the properties of graphene is not retained. This is because some of the sp^2-hybridized carbon atoms become sp^3-hybridized when reacted with oxygen to form carboxylic groups, epoxy groups and hydroxide groups. The changes in the sheets create structure defects like holes which causes disruption in the continuation of sp^2-hybridized carbon atoms [21]. Properties that change are for example the hydrophobicity, thermal and electric conductivity, appearance and many more. Because of an interrupted sp^2 hybridized basal plane GO becomes more insulating than graphene. [22, 23] However GO sheets do not aggregate with each other with as strong van deer Waals forces as graphene sheets since the oxide groups repel each other. The functional oxide groups enables grafting and functionalization of the GO with polymers. [13, 23] In contrast to the graphene that is pure hydrophobic does the structure of GO differ in hydrophilic and hydrophobicity. The edges where the carboxylic groups are located are of a more hydrophilic nature than the basal plane which contains epoxy and hydroxyl groups. [24] Some of the lost properties created by oxidation can be repaired by reduction of the oxide groups to reduced graphene oxide, (RGO). An example of the RGO structure can be seen in Figure 5. [21]

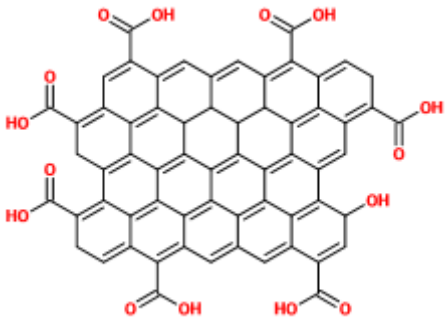

Figure 5: One version of RGO. After Graphenea [25]

The carbon/oxygen ratio in GO is between 4:1 and 2:1 while the ratio for RGO can vary from 10:1 and up to around 246:1 depending on how effective the reduction method has been. [21, 26] RGO and GO also differ in physical appearance in water dispersions, GO has a light yellow/brown color while RGO is darker [27]. The optical differences between GO and RGO and graphene depends on the level of sp^2 hybridized carbon which absorb light to a larger extent than sp^3 hybridized carbon [28].

Reduction Processes of Graphene Oxide

There are many ways of reducing GO. The main routes are chemical, thermal and electrochemical. The most common method uses hydrazine hydrate in a chemical reducing procedure. More environmentally friendly reducing agents are glucose, fructose or vitamin C [27, 29]. Other possible reduction procedures are different irradiation mechanisms like microwaves or phonon irradiation. During reduction processes are the epoxy and hydroxyl groups primarily reduced while the carboxylic and carbonylic groups are maintained because they contain higher energy. [21]

Reduction can also be made when the film has already been applied on a substrate by hydroiodide acid. This method is promising because it has been proven that this procedure gives fewer imperfections on a film than by vitamin C and temperature reductive processes. [30]

2.2.3 GRMs in Anti- corrosion Coatings

GO and RGO will hereafter be collectively denominated graphene like materials, GRMs. When graphene is oxidized to GO the properties are not maintained but the oxidation creates more bonding sites for grafting polymers [21, 28]. By incorporating RGO and GO in coatings makes it possible to adhere GRMs to different substrates. However in one investigation by Su Y. et al the adhesiveness is stronger to polymeric substrates such as (PET) than to metals. The adhesive ability is also reduced when the oxygen content is reduced and the film also becomes more brittle. [30] Adhesiveness is the property where substances of different nature stick together for example a particle sticking to the substrate. Cohesiveness is on the other hand the property where substances of the same nature stick together like a polymers of the same kind that interact and crosslink with each other. [31] To be able to get GRMs to adhere to a surface of metal adhesive polymers can be used or by incorporating GRMs in binders or it can be grafted with adhesive polymers. Depending on the polymer system used either the GRM or the polymer may need to be functionalized with functional groups that can interact with the other part of the nanocomposite. [32, 33]

2.3 Grafting

To be able to immobilize fillers and additives, they can be grafted with a polymer. Grafting can be made by “grafting to” and “grafting from”; grafting to is when a polymer is reacted into a substrate surface or a backbone polymer which can be seen in Figure 6. Grafting from is when initiators are immobilized on the surface of a substrate and the monomer reacts and polymerize. To be able to graft a solid surface it should contain functional groups such as for example hydrolytic, carboxylic or amino groups. [33, 34]

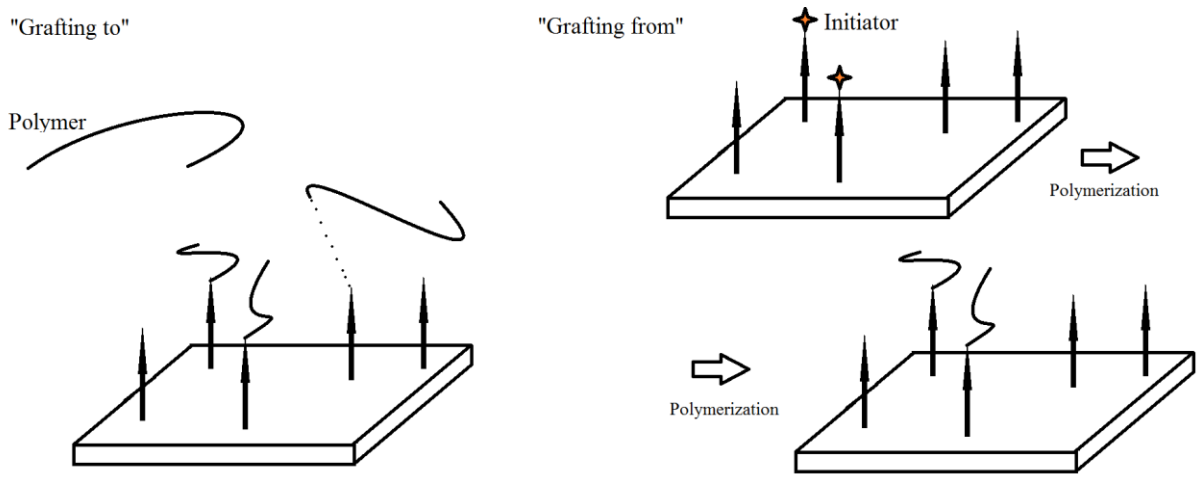

Figure 6: A simplified picture over the “grafting to” and “grafting from” methods. After [34]

To be able to modify the surface properties of a solid it is possible to bind polymers covalently to the functional groups on a solid surface. A polymer can be grafted covalently or non-covalently to a solid by adsorption and by chemical reactions. [33] By grafting GRMs it is possible to facilitate dispersion of GRM in the polymer matrix by creating steric hindrance between the graphene sheets.[18]

Properties that can be modified by the use of graphene are for example thermal conductance. Some studies have investigated the thermal influence of using graphene as filler in a polymer to increase the thermal properties of polymers that are inherently poor compared to crystalline materials. [32, 35]

GRMs has reportedly been grafted with among others polystyrene, epoxy, polymethylmethacrylate, polypropylene just to mention a few. Studies of polyaniline grafted GRMs used in-situ polymerization of aniline to the GRM sheets which is a kind of “grafting from” method.[18, 33]

2.4 Thermal Conduction and Heat Transport

The property of thermal conductivity is the ability to transmit heat through the material matrix driven by a temperature gradient; this can be seen in Figure 7. When a material conducts heat, the atoms in the matrix vibrate. When atoms in the matrix vibrate to equilibrate the temperature gradient phonons, energy packages, are sent through the matrix. Depending on the material structure the heat conducting property is of different magnitudes. In solids the atoms are strongly bound to their neighbours which limits the degree of vibration. The solids with the highest thermal conductivity are those that have a diamond like structure. [36] In liquid solutions and dispersions the vibrations is not hindered to the same extent as in solids. However, for this case, a continuing solid matrix does not exist for the phonons to be sent through which generally decreases the thermal conductivity compared to solids.

Figure 7: The temperature conductance. After [37]

Because of the natural tendency to strive for equilibrium, heat is transported from the higher energy content, warm medium to the lower energy content cold medium. One dimensional heat transport in steady state can be described by Fourier's law. [37]

$$q = -k\frac{dT}{dx} \qquad \text{Equation 1.}$$

Where q is the heat flux and *k* is the heat conduction constant, which is an individual constant for every material. [37]

Polymers generally have very low thermal conductive properties in comparison with metals. Some examples are showed in Table 1. By adding a conductive filler or additive the thermal conduction can be increased. One additive can for example be graphene that according to Serov A.Y. et al has a "*high in-plane thermal conductivity*" [38]. Despite that pure graphene has excellent thermal conduction the heat conduction of the nanocomposite may not increase a great deal with the presence of graphene. This is due to the graphene/polymer interface which has a resistance to the lattice vibration and phonon transportation that the thermal conduction depends on. This resistance effect is called Kapitza resistance.[39] The Kapitza resistance can be diminished by an increasing the filler contnent which improves the chance of the filler to be in contact with each other which then increase the thermal conduction. However by adding fillers, other thermal properties, for instances the melting point and glass transition temperature can change for the polymer/filler composite. [40, 41] The glass

transition temperature is a temperature range where a polymer becomes solid and stops moving freely which is dependent on the chains flexibility, structure, molar mass, and cross-linking. [41]

The thermal conductivity of GO is not as effective as for graphene and the "true value" is still unknown. Nevertheless there are several studies where the thermal properties of GO and RGO have been compared, both theoretically and practically. The results were very different but the conclusion is quite similar, which reveals that reduced oxygen content improved the thermal conduction. [42, 43]

Table 1: Thermal Conductivities of GRM and Other Materials

Substance	Thermal conductivity in room temperature W/mK	Method	Reference
Pristine Graphene	1500 – 5800	Theoretical	[43]
Stainless Steel	11-21	Unknown	[44]
Polyaniline	~0.6	At 25^{o}C, "E-type differential thermocouple"	[45]
RGO after Hummers method	0.14 -2.87	Electrical measurement in several points	[42]
RGO, 5% oxygen	28	NEMD (theoretical)	[43]
RGO, 0.5% oxygen coverage	50% of Pristine Graphene	NEMD (theoretical)	[43]
Poly Styrene	0.17	Unknown	[46]
Polymethylmethacrylate	0.17-0.19	Unknown	[46]

2.5 Dispersion

Dispersion is defined as one phase, the solute particles, evenly distributed in another phase, the solution. The particles are exposed to several forces; the overall forces are gravitational forces, viscous drag forces and random Brownian motion which is caused by the kinetic energy of the solute. The individual particles also experience attractive van deer Waal forces and electrostatic forces. In dispersions, the particles have an overall charged surface which attracts opposite charged particles in the dispersion and creates a double layer. [47]

One way of evaluating the colloidal stability is to measure the zeta potential. The zeta potential describes the interaction between the solute and solution particles. [48] By evaluating the zeta potential the potential of the outer limit of the double layer also called the slipping plane are measured [49]. The procedure of evaluating this potential can be by measuring the velocity at which the solutes moves across the dispersion towards an opposite charged electrode during the impact of an electrical field. During the applied field the particle velocity is limited by the solution particles that cross the slipping plane. This limitation is constant and proportional to the zeta potential. [47]

Particles with dissimilar charge attract each other, while those with the same charge repel each other electrostatically. The stability of these electrostatic stabilized dispersions can be understood and investigated in the context of the distance between particles. This is described in DVLO theory where the distance is shown as a function of energy, eV, which can be seen in Figure 8. Particles in these dispersions have a critical distance where the particles aggregate, due to that the attractive forces rule over the repulsive forces. [47] It should be noted that particles can also be sterically hindered from close enough contact for aggregation, for example by dispersants attached to the particle surface.

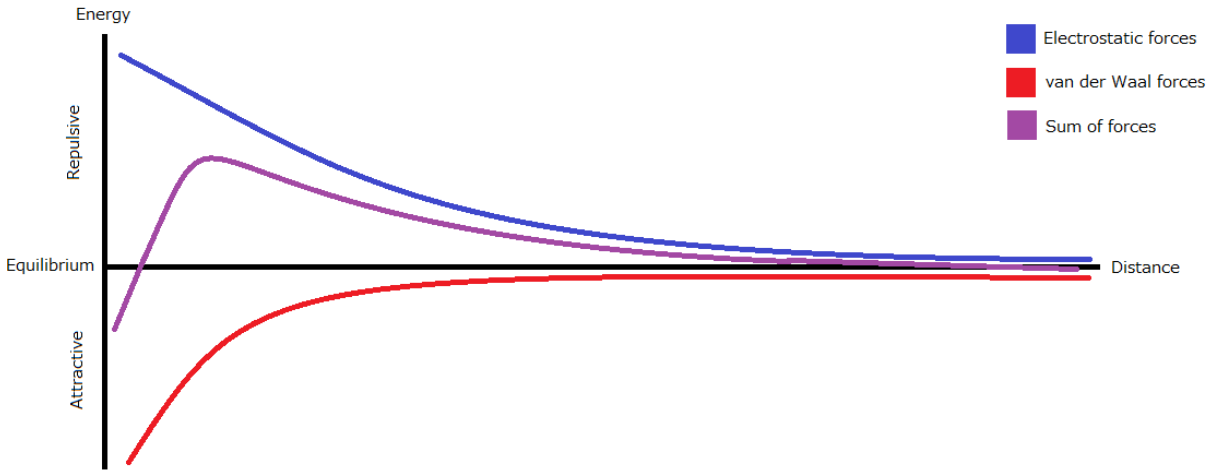

Figure 8: The DVLO theory. [47]

One way to solve poorly dispersible substances in a solution is by adding surfactants. Surfactants consist of hydrophilic and hydrophobic parts which can act as “bridges” between the particle and the solvent. The solvent choice is important to make the dispersion as effective as possible by increasing the width of the double layer and increase the repulsive forces between the particles. The repulsive forces can also be increased by grafting the

particles with polymers that act as a steric hinder for aggregation. To choose a good surfactant/dispersant of polymer to graft onto the particle, the part protruding into the solvent should be as compatible to the solvent as possible. [47]

How well a solvent will disperse a solute/ part of dispersant/polymer and which mechanism that will be the dominant one can be estimated with Hansen's solubility parameters. Hansen's solubility parameters are the following three parameters: polarity δ_P, dispersion δ_D and hydrogen bonding δ_H. These can be calculated by Equation 2. [22, 41]:

$$\langle \delta_i \rangle = \frac{\sum C * \delta_i}{\sum C}, i = P, H, D \qquad \text{Equation 2.}$$

where C is the concentration of solute dispersed in the chosen solvent.
The total cohesive force in the solution is the sum of the affecting mechanisms seen in Equation 3. [41]

$$\delta = \sqrt{\delta_P + \delta_H + \delta_D} \qquad \text{Equation 3.}$$

2.5.1 Dispersing Graphene

Graphene is hydrophobic, which makes it poorly soluble in water. The dispersion in water can be improved by oxidizing the graphene sheet to GO. The polar oxide groups on GO makes it possible to keep the sheets separated and stabilized in organic polar solvents. The surface energy of the solvent molecules should have similar surface energy as the graphene or GO to be able to successfully separate the sheets. Solvents that have successfully been used in other investigations are N-methyl 2-perrolidone (NMP), dimethylformamide (DMF) and dimethylacetamide (DMA). All of these can be seen in Figure 9. [32, 50]

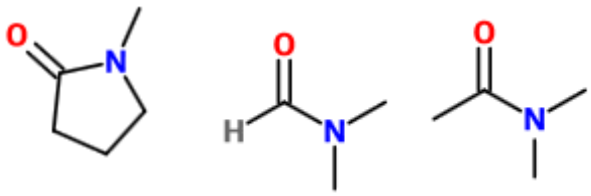

Figure 9: (from left to right) NMP, DMF and DMA [51]

Currently it seem that the most commonly used solvent is NMP which have many advantages such as high boiling temperature and according to Bracamonte, et al it does not leave any physical traces as it dries. [52]

The effectiveness of changing the properties of polymers with graphene in a nanocomposite is dependent on the dispersion level of the graphene in the polymer and the cohesion of the nanocomposite [53]. The amount of filler is limited by the interactions between an additive and its surrounding matrix. The critical amount where the particles experience long-range connectivity occurs, and for example the viscosity increase with the particle concentration increases rapidly is called the percolation threshold [13, 54].

Pristine graphene is inert but can influence polymer chains in a polymer matrix by non-covalent bonds. When graphene is oxidized the graphene becomes able to interact by its substituents with the surrounding polymers which facilitate the dispersion stability. [13] By using surfactants when grafting graphene the polymers can be evenly dispersed on the surface of GO. One surfactant used in literature is cetyltrimethylammoniumbromide, CTAB [55].

Another factor affecting the dispersion of GRM's is pH. GRM's, i.e. GO and RGO, contains carboxylic substituents which becomes negatively charged in alkaline environments. The deprotonation of GRMs increases the zeta potential which increase the stability of the dispersion. [50] According to B. Konkena et al. the most stable solutions of GO are at a pH greater than 4 and for RGO at a pH greater than 8.[56]

2.6 Polymers for corrosion protection

Intrinsically conducting polymers, ICPs, have quite recently been receiving attention for corrosion protection applications. The conducting property makes it possible to transport electrons through the polymer and even out the anodic and cathodic processes. Doped polyaniline is one example of an ICP. A comprehensive literature study about polyaniline as a protective film for corrosion inhibition has critically evaluated three possible mechanisms: physical barrier, chemical inhibition and as an "anodic protector". The conclusion of the investigation was that the physical and chemical inhibition mechanism could not be supported; however the anodic protection was theoretically satisfactory to some extent. [7]

2.6.1 Polyaniline

Polyaniline has received a great deal of attention for the corrosion inhibition applications because the easiness to polymerize in ambient temperatures, its environmental stability and its conducting ability [57]. Polyaniline exists in three different forms: leucoemraldine which is a reduced form, pernigailine which is an oxidized form and the emeraldine form which has a structure which is partial oxidized and partial reduced. The emeraldine form can be in an insulating base form and as a conductive chemically charged salt form. All polyaniline forms mentioned above can be seen in Figure 10. [58]

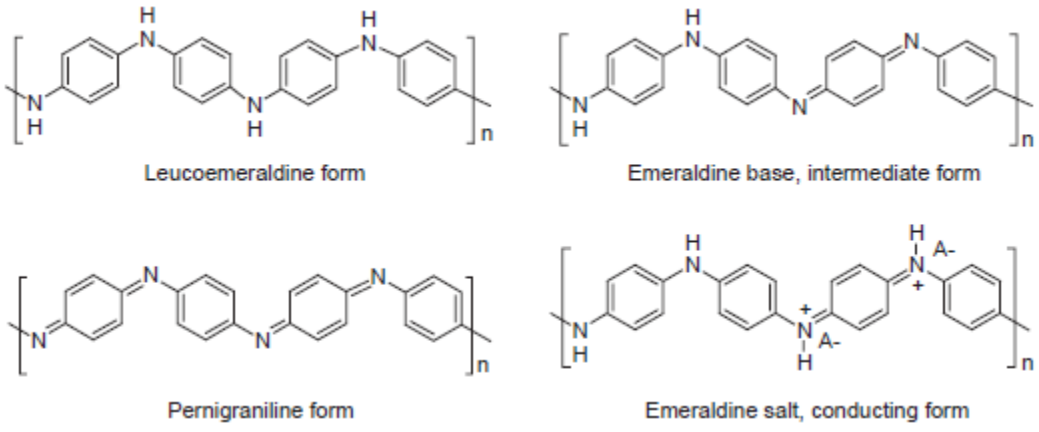

Figure 10: The four different states of polyaniline. [7]

The conducting form is the one that should be used for corrosion inhibition applications for steels and other metals. It has however been discovered that the top layer of the coating of emeraldine salt can be reduced to leucoemeraldine when put in an alkaline environment. This can be prevented by insulating the coating with a non-conducting top coating. [7]

The emeraldine form can be transformed between the base and salt form by a doping and de-doping, which also can be seen as a self-healing effect [7]. If polyaniline is used on a metal the self-healing mechanism together with the oxidizing properties of the polymer leads to corrosion passivation of the substrate [59].

Polyaniline is produced by dispersing aniline monomers in a strong acid, often HCl, and then add an oxidizing initiator like ammonium sulfate. The reaction is exothermic so the reaction vessel is often put in an ice-bath. The pH of the acid and the way of adding the initiator, all at ones or slowly, influence the final appearance of the polyaniline. [60]

Aniline is dispersed in a strong acid because it is immiscible in water but by protonating the amino-group the dissolution is facilitated. Aniline is a weak base with a pK_b value of 9.4 which gives a pK_a value of 4.6 see Equation 4 which means that 50 % of the aniline monomers are protonated at the pH of 4.6. [61, 62]

$$pK_a + pK_b = 14 \qquad \text{Equation 4.}$$

2.6.2 Polymer/graphene Nanocomposite

Polymers can be put on a substrate to increase the corrosion protection and as described previously in section 2.1, there are many corrosion mechanisms that a polymer can affect. The barrier effect, as an example, of a polymer has in previous studies been improved by creating a nanocomposite with graphene. In current industrial applications clay particles can be used for the same purpose. Previous studies about graphene as a barrier were compared to clay particles and the results were that graphene was more effective as a barrier than clay particles. Thus by adding graphene to a polymer the total barrier effect of the coating increases. [14, 63]

A study by Yu et al about a polystyrene/graphene nanocomposite showed an increased barrier effect by adding graphene to the polystyrene matrix compared to pure polystyrene. The graphene amount added was 2wt%. [64]

Graphene has in several reports been grafted with polyaniline as a corrosion inhibitor on steel. The final PAni/graphene coating are claimed to be environmentally friendly, stable and when mixed with an adhesion epoxy aid it had good adhesive properties to steel. The polymer matrix in combination with graphene resulted in a longer diffusion pathway for corrosive molecules like water, oxygen and salt. [14] The disadvantage with polyaniline and also with graphene is the difficulty to disperse the end product. This problem was resolved by addition of a surfactant to the polymer mixture, for example cetyltrimethylammonium bromide, CTAB. [56] The most commonly used solvent for dispersing polyaniline graphene is N-methyl- 2- pyrrolidone [57].

Another study made by Chang et al used an epoxy graphene nanocomposite in combination with templating a surface structure to create a super hydrophobic coating on cold rolled steel. The super hydrophobicity was shown by a contact angle of 150^{o} or more on the sample. The graphene from exfoliation of graphite, was oxidized, reduced and dispersed in a solvent. The amount of reduced graphene used was 1wt%. The electrochemical tests of the coating showed that the anticorrosion property increased. Investigated in the report was also that the contact angle was constant for all the 30 days it was tested. [63]

2.7 Analyzing Methods

2.7.1 Raman Spectroscopy

During Raman spectroscopy a sample is irradiated with a high energy laser beam. The contributed energy induces the dipole moment by vibrations that excite the electrons to different levels. This makes it possible to see different kinds of bonds in the sample since the bonding vibrate to different extends. [65]

The resulting Raman scattering contains three different reflected scatterings. The largest one is the Rayleigh scattering which has the same frequency as the incoming laser light. The other scatterings are Stokes and anti-Stokes. Stokes scattering is the reflected light from the ground vibration level and anti-stokes is light scattered from the annihilation of excited electron. The Stokes scattering is usually used for analysis with Raman spectroscopy. [65]

Raman spectra for graphene contain three main peaks and sometimes four depending on if the graphene matrix are defected or not. The three main peaks are called the D-, G- and 2D-band which stands for the vibrations from sp^3, sp^2 and multiple layers see Figure 11. The appearance of the D-band in the Raman spectra of graphene is only related to the edges where the graphene sheet cannot contain the sp^2 structure. The locations of the three characteristic bands in a Raman spectra is 1300 cm^{-1} for the D-band, around 1600 cm^{-1} for G-band and around 2700 for the 2D band. If the 2D band is high and broad the analyzed particle does probably contain more than one layer of graphene. [66, 67]

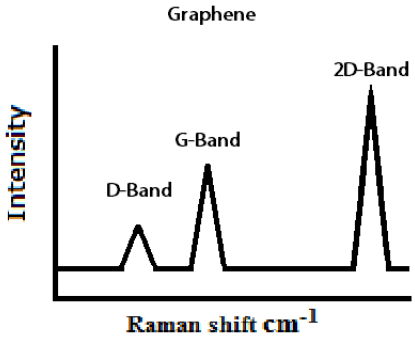

Figure 11: A simplified picture of a Raman spectroscopy of graphene. Made after [66]

The Raman spectra for GO differ from graphene. The ratio between the D and G band is much lower because graphene oxide contains of both sp^3 and sp^2 hybridized carbon. The 2D band cannot be used for the investigation of the number of layers because the 2D band are in this case hard to identify in the presence of several peaks from the carbon bonding to oxygen groups see Figure 12. [68]

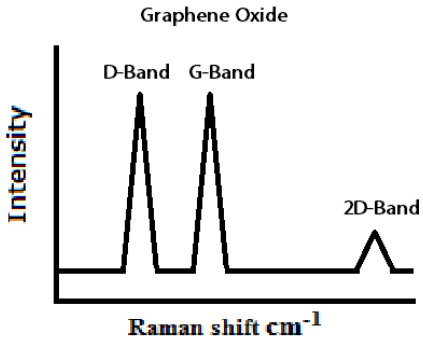

Figure 12: A simplified picture of Raman spectrum of GO. Made after [68]

2.7.2 Scanning Electron Microscopy, SEM

In this kind of electron microscopy electrons are accelerated between the electron emitting cathode which can be a heated tungsten filament and an anode. The monochromatic electron beam is then focused onto the sample surfaces through condensing and objective lenses. The energy from the beam makes the electrons from the atoms at the surface of the investigated sample to either escape from the surface or be adsorbed. The escaping electrons are collected by the detector that amplifies them and creates a electron micrograph. In the lighter parts of the image more electrons have been captured by the detector when irradiated that specific area of the specimen. Information acquired from this technique is surface knowledge like defects, morphology and particle size. [69]

2.7.3 Transmission Electron Microscopy, TEM

Transmission electron microscope has higher resolution than the scanning electron microscope because electrons with significantly higher energy can be generated from the cathode. This microscope has a similar construction as scanning electron microscope with condensing lenses, an objective lens and intermediate lenses. Samples analyzed by the transmission electron microscope are very thin, which makes it possible for the electrons to pass through the sample and by that create an image showing atom position under suitable conditions. [69]

2.7.4 Atomic Force Microscopy, AFM

In AFM properties such as topography, friction, elasticity, adhesion can be investigated by the usage of a flexible cantilever with a sharp tip at the downside. The upside of the cantilever that doesn't face the surface is irradiated by a laser beam which is reflected towards a photodiode detector. The tip is very close to the surface atoms and depending on the repulsion or attraction to the atoms the cantilever flex away or against the surface. There are two principle modes of analysis; one is the static contact mode where the tip is held a distance from the surface where the repulsive forces dominate. The tip is dragged along the surface to measure the height difference. The other mode is the dynamic non-contact mode where the tip is held at a distance where the attractive forces dominate. In this case, the cantilever oscillates and the difference in the oscillation frequency and amplitude of each point measured are used to create a three dimensional image of the surface. [69]

3. Experimental

3.1 Graphene Like Materials, GRM

3.1.1 Analysis of GRMs

Materials

Chemical	Concentration	Supplier	pH
Water dispersed graphene oxide, GO_W	4 mg/ml	Graphena	3
Water dispersed, ammonium functionalized graphene oxide, AGO	1 mg/ml	Sigma Aldrich	6

Elemental analysis from supplier [%]		
	GOw	AGO
Carbon	49-56	40-50
Hydrogen	0-1	
Nitrogen	0-1	3-6
Sulphur	0-2	≤3
Oxygen	41-50	

The structure of AGO can be seen in Figure 13.

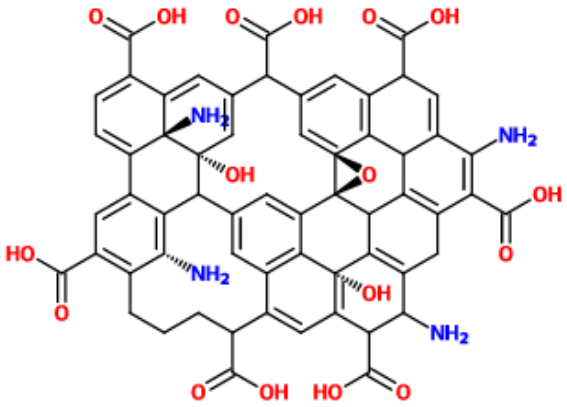

Figure 13: A representation of AGO after suppliers' home page. [70]

Materials used
Glass slides
SEM aluminum pins
Mica slides
Disposable cuvettes
Ultrasonication bath

Instrumentation and sample preparation:

I. Raman spectroscopy; to investigate the relationship between sp^3 and sp^2 hybridized carbons. The samples were prepared by putting a drop of either of the samples GO_W and AGO on a glass slide and leave until the water had evaporated. The Raman data was analyzed by the software Origin 9.1 which is a raw data program and the graphs in appendix are made in Matlab 2013b. The Raman measurements were made by single spectra at three to five places at the samples and a mean value was then calculated which are represented in the results.

II. SEM; to investigate the GRM sheet size and appearance. A drop of the sample was put on a SEM pins and left to dry in a fume hood for a few hours before analyzed by SEM.

III. AFM; for investigation of the sheet height. The GO and AGO was diluted and a drop of the dispersion was put on mica which was left to dry in a laminar flow before analyzed. The AFM images has been flattened in the 3rd order and cleaned from spikes and streaks by using a cutoff of 3 nm with the software Nanoscope Analysis 1.5.

IV. Nanosizer; were used for measurement of the general particle size. The samples were diluted with distilled water and put in a cuvette and then analyzed in the Nanosizer instrument. The effect of ultrasonication bath on the level of dispersion was investigated briefly. For the "long time" sonication test of AGO three samples with approximately the same concentration of 0.5 mg/ml, were treated the same and tested in the Nanosizer.

Instruments:

Instrument	*Maker*
Raman spectroscopy	*WITec alfa300 RAS, LASER 532 nm*
SEM	*FEI modell Quanta FEG 250*
Nanosizer	*Malvern Instruments*
AFM	*Bruker Microscope V*

3.1.2 AGO Dependence on pH

Chemical name	Formula	Supplier	CAS
Hydrogen Chloride	HCl	Sigma Aldrich	9004-54-0
Sodium Hydroxide	NaOH	Sigma Aldrich	1310-73-2
AGO	$C_nH_mO_xN_y$	Sigma Aldrich	-
Distilleds Water	H_2O	-	7732-18-5

Materials used	Maker
Electronic pH-meter	Mettler Toledo
Glass vessels 5 ml	
Pipets 1-1000 µl	
Ultrasonication bath	

Water solutions of different pH were made. Acidic solutions were created by adding HCl to distilled water. The alkaline solutions were made by adding NaOH to water. The pH of the solution was measured with an electronic pH meter. When the target pH was reached, 400 µl of the solvent was mixed with 2 µl of the 1mg/ml AGO and put in an ultrasonication bath for 3 minutes. The concentration of the resulting mixture was 0.005 $\frac{\mu g}{\mu l}$ AGO.

3.2 Polyaniline

Chemicals

	Chemical name	Formula	Supplier	CAS
Reaction	Hydrogen chloride	HCl	Sigma Aldrich	9004-54-0
	Aniline	$C_6H_5NH_2$	Merck Schuchardt	62-53-3
	Ammonium persulfate	$(NH_4)_2S_2O_8$	Scharlau	7727-54-0
	AGO	$C_nH_mO_xN_y$ [54]	Sigma Aldrich	-
	NMP	C_5H_3NO	Sigma Aldrich	872-50-4
Cleaning	Distilled Water	H_2O	-	7732-18-5
	Methanol	CH_3OH	Fisher lab	67-56-1

Materials

Reaction	Cleaning Procedure	Analyzing instruments	
		Instrument	Maker
Measuring cylinder	Filter paper	SEM	FEI
50ml beaker	Ceramic strainer	Nanosizer	Malvern
Cooling bath at 0°C	Filter tube	TEM	
Syringes 1 and 5 ml	Round bottle 50 ml	AFM	Bruker
Magnetic stirrer	Soxhlet tube 30 ml	Raman spectroscopy	WITec
Ultrasonication bath	Cooling tube	PH electrode	VWR
Rubber Cork	Heating plate with a magnetic stirrer		

Original Method

20 ml of 0.1 M HCl was poured into a 50 ml beaker which was put in a cooling bath at 0 °C. 2 ml of 1 mg/ml AGO was added to the beaker and a rubber cork was put on the beaker before 200 µL of aniline was carefully added with syringe to the cold HCl, which gives an aniline concentration of 0.01 M. When aniline was added the aniline and AGO formed a cluster which sank to the bottom of the reaction vessel.

480 mg of the initiator $(NH_4)_2S_2O_8$ was dissolved in 2.5 ml distilled water. Half of the initiator volume was added by syringe to the mixture. After a reaction time of 6 hours a second portion with the other half of the initiator was added to the reaction and left over night. The mixture becomes dark green which is an indicator that emeraldine salt has been formed. The product is a precipitation which makes it easy to extract the product by filtration.

The product was cleaned by folding the filter paper with the product and put in a filter tube which in turn was put in a Soxhlet extraction apparatus with distilled water. The temperature of the water was set to 140°C to make the water evaporate into the Soxhlet trap. The evaporation of water was performed for 24h. After 24 h the water was shifted to methanol and the temperature was set to 80°C and left for another 24h.

The dry product was dispersed in NMP using ultrasonication.

Approximated time needed for analysis and cleaning was 72 hours.

3.2.1 The Reference

There was a reference sample of PAni AGO made according to the general method at SP with 20wt% AGO. This sample will be named PAni/AGO-0. An amount of 0.076 g of the dried sample was dissolved in 10 ml NMP which gives a concentration of 7.6 mg/ml. The product was analyzed by Raman spectroscopy, AFM, TEM and SEM.

3.3 Binders

Because the PAni/AGO particles demonstrate poor adhesion to the stainless steel substrate, it needs to be incorporated into a polymer coating or use polymers as adhesion aids.Three commercial binders, choosen for their good anti-corrosion properties, were investigated for this purpose.

3.3.1 Commercial Water Based Binders

Three commercial binders were tested.

Name	**Polymer**	**Emulsion medium**	**Dry weight**	**Supplier**
ENCOR 2433	Acrylic	Water	50%	Arkema
Xynopol AO 551L	Vinyl esters Acrylate	Water	50%	Xyntra
Xynopol AO 557L	Vinyl esters Acrylate	Water	50%	Xyntra

Stainless steel pieces were coated with each binder and sent to a project partner to be tested in the given application.

The binders were combined with a GO_W load of 0,6 wt%.

Encor was also combined with GO_w in the loadings stated in Table 2.

Table 2: The vol% and wt % of GO_W added to the commercial binder Encor.

Sample	Vol % GO_W	Wt% GO_W
1	50	1,14
2	60	1,56
3	70	2,42
4	80	4,16
5	90	9,35

4. Results and discussion

4.1 Graphene like materials, GRMs

4.1.1 Analysis of GRMs

Raman spectroscopy

The intensities and relationships between the D-band (sp^3) and G-band (sp^2) can be seen in Table 3. The result varied slightly between the primary products.

Table 3: The D- and G- band relationship from the Raman spectra of the primary products

GRM	I_D	I_G	I_D/I_G	I_D+I_G	$I_D/(I_D+I_G)$	$I_G/(I_D+I_G)$
GO_W	56.8	61.4	0.93	118.3	0.48	0.52
AGO	105.7	102.2	1.03	207.9	0.51	0.49

The peak placement of the D and G band is the same for the two products which can be seen in Figure 27 and 28 in the appendix. The D band is placed around 1350 cm^{-1} and the G-band around 1600 cm^{-1}.

The Raman spectroscopy showed the characteristic peaks of GO for the primary products. For AGO in Figure 28 in appendix there is a peak at 1100 cm^{-1} that appears. This peak is probably a glass peak from the glass substrate.

The sp^3/sp^2 ratio is 0.11 or 12 % higher for AGO than for GO_W. This means that the amount of sp^2 hybridized carbons is larger than the amount of sp^3 hybridized carbons, which probably is because of the addition of ammonia groups to the GO sheets in AGO. The Raman spectroscopy of GO_w in Figure 28, have more separated peaks than AGO in Figure 28. This can be caused by the addition of NH_2 in AGO, which can have a signal peak between the two central peaks.

SEM

The SEM image, seen in Figure 14 below, shows a large variation of size and shape of the GO_W and AGO sheets. The size distribution in a single drop of the GO_W is estimated to be between 1-7 µm and for AGO it's larger than 10 µm. The micrograph also shows that one drop of GO_W with concentration of 4 mg/ml is a large amount of GO_W sheets despite its low concentration. The AGO also tends to fold more and are darker than GO_W.

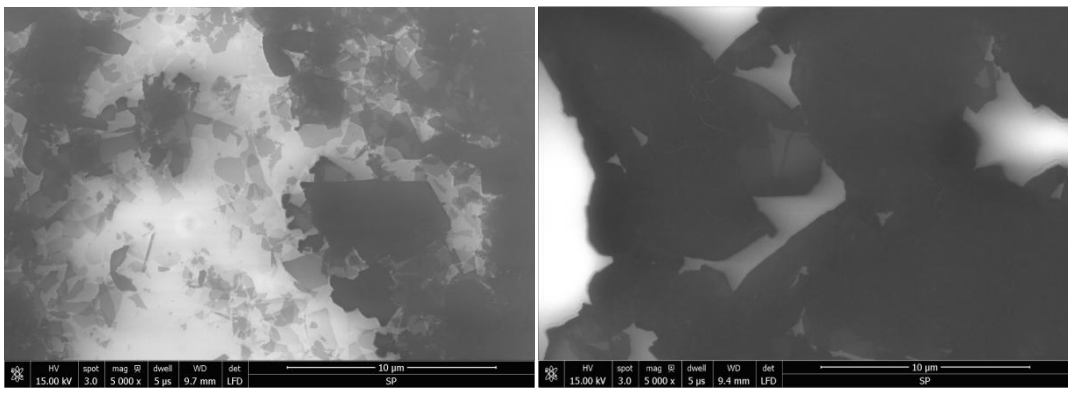

Figure 14: SEM micrograph of GO_W (left) and AGO (right) by A. Dahlman. The scale bar is 10 µm.

AFM

In diluted samples of GO_W and AGO, single sheets were observed in the AFM. The height of the flake was between 1-2 nm, see Figure 15 and 16. The irregularities in the GO_W sheet image could probably be caused by folding in the sheets.

The height measurements of the flake were made by measurement of the height difference from the mica substrate of the GRM sheet surface. The measurement points at the edges of the flake, can be seen by the markings in the Figures 15-16. Figure 15b shows how the surface height varies and the table in 15c lists the numerical value of the height of the GRM sheet. As can be seen the surfaces of both the substrate and GO sheet are very smooth. The point chosen for the numerical analysis were taken at the highest point at the edge.

The mean value of the thickness measured in three points of a flake was approximately 1.62 nm for GO_w and 1.39 nm for AGO. The height of the GRMs is slightly higher than for pristine graphene which have a thickness of 1 nm as described in section 2.2.1.

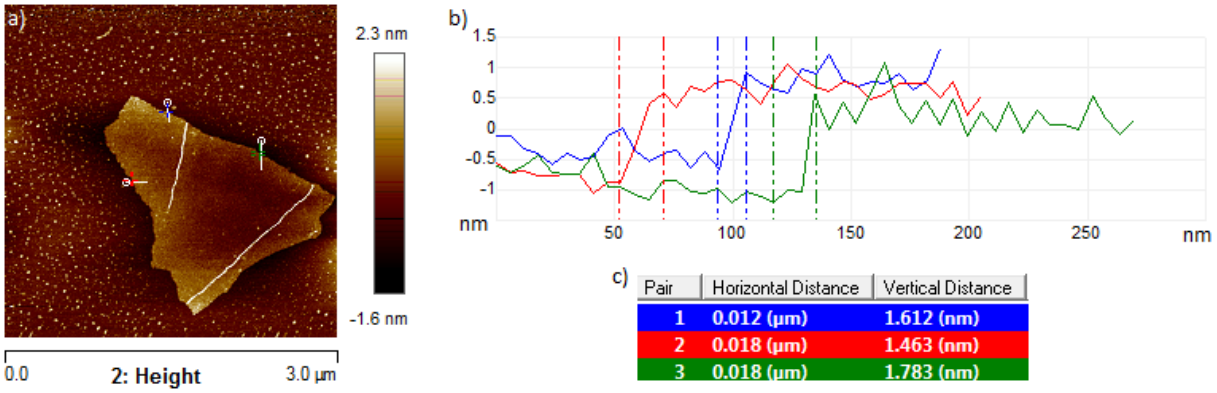

Figure 15: The AFM result of GO_W, a) the AFM image of a GO flake with three measure at points indicated heights measurements, b) the line scans of the defined by marks in a, c) the vertical distances result marked in b, see the color codes.

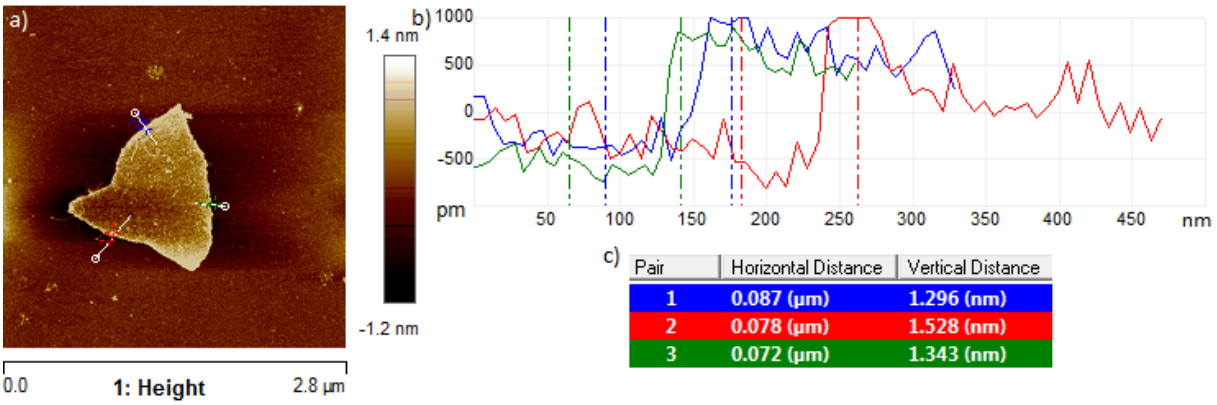

Figure 16: The AFM result of AGO, a) the AFM image of one AGO flake, b) three measured heights, c) the heights in nm.

Nanosizer

The particle size and how the particle size change when exposed to ultra- sonication of GO_W and AGO dispersions in water were investigated use of the Nanosizer. After brief ultrasonication, both the GRMs experience a distinct decrease in the average particle size seen in Table 4. After a short time lapse the particles size decreased even more, probably because the oversized particles sank to the bottom due to a rapid sedimentation. GO_W was even analysed after a sonication time of 15 minutes. The decrease was not as distinct as after the first 5 minutes, which probably means that most of the flocculated flakes had already been broken up.

Table 4: Short Time Sonication of GRMs

Ultrasonication time [min]	**Average size [nm]**	
	GO_W	**AGO**
0	1840	157400
5 (direct after)	883	2300
5 (5 min after ultrasonication)	852	1520
15	838	N/A

AGO was subjected for longer ultrasonication times, between 0.5-1.2 h. The result of long time sonication of AGO is presented in Figure 17 and demonstrates that too long ultrasonication does not improve the particle size rather the opposite. The pattern does not seem to be conclusive because the size varies drastically.

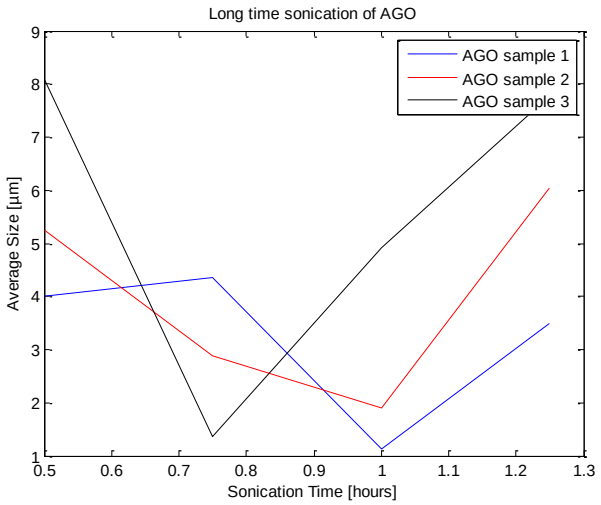

Figure 17: Long sonication time of AGO

Sonication is used to disperse aggregated AGO sheets. The large increase at the end of the measurement can be due that the exfoliated sheets are moved closer together by the inserted energy by the sonication.

AGO dependence on pH

The AGO level of dispersion in different pH were investigated by diluting distilled water with HCl and NaOH, respectively. 400 µl of the target pH were put in a bottle and 2 µl of 1 mg/ml AGO which is a water dispersion were added to the bottle.

AGO was best dispersed at a pH between 4 and 6. At low pH there were big clusters of AGO and at higher pH a lot of the AGO sank to the bottom. This conclusion could be reached by visual observation of the dispersion colour of AGO at different pH, Figure 18. At low pH large clusters of AGO were formed and these had lower density than the water, as most of the particles floated on the surface of the dispersion. At pH higher than 6 the particles did not form clusters but they were less well dispersed than at pH 4-6. There are still some large particles in the darkest samples but is still less than in the other vessels. The level of dispersion would most likely improve the dispersions were ultra-sonicated.

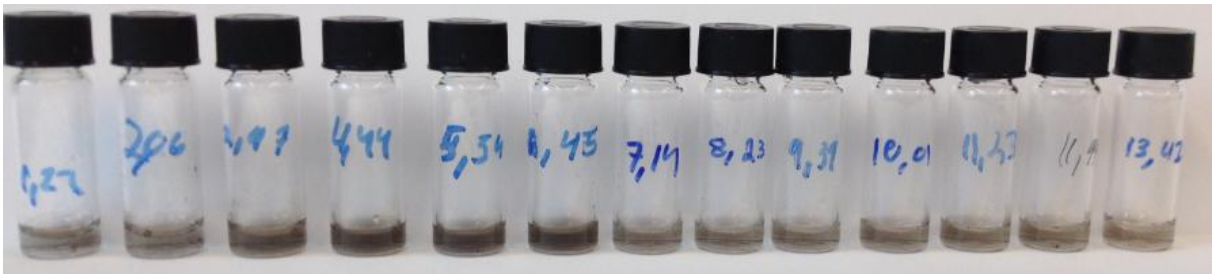

Figure 18: AGO in different pH solutions between 1.22 -13.42.

The pH dependent behavior can be caused by the different in properties at the edges and the base plane of GO described in section 2.2.2 [25]. In addition AGO has alkaline aminogroups which has a basic nature. The industrial produced GO_W solution has a pH of 4 which mean that oxygenated graphene has a higher amount of acidic groups than basic. The industrial produced AGO has a pH of 6 which is closer to neutral pH which could indicate that the acidic/basic ratio is closer to one than for GO_W assuming that these dispersions have not been adjusted for pH by the supplier.

4.2 Polyaniline

4.2.1 AFM and TEM of 20 wt% AGO

AFM

The batch PAni/AGO-0, containing PAni and an AGO load of 20wt% were put on a mica plate and were dried in a fume hood during the night before analyzing by AFM. The particle location can be seen in Figure 19. The height of the largest particles and thus lightest particles in the image is between 20 and 37 nm.

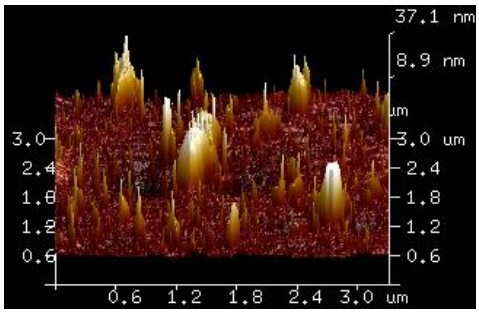

Figure 19: PAni/AGO-0 particle location on the mica substrate.

The adhesion and deformation were analyzed by the AFM. The micrographs in Figure 20 show the adhesion to the left and deformation to the right. In the adhesion image the lighter parts are the more adhesive ones, and in the deformation image the darkest parts of the image are the most deformable. The resulting AFM micrograph in Figure 20 shows that the center particle, the large particle in Figure 19, has non-uniform adhesiveness. Its deformation varies slightly across it as well however the overall deformation possibility is low.

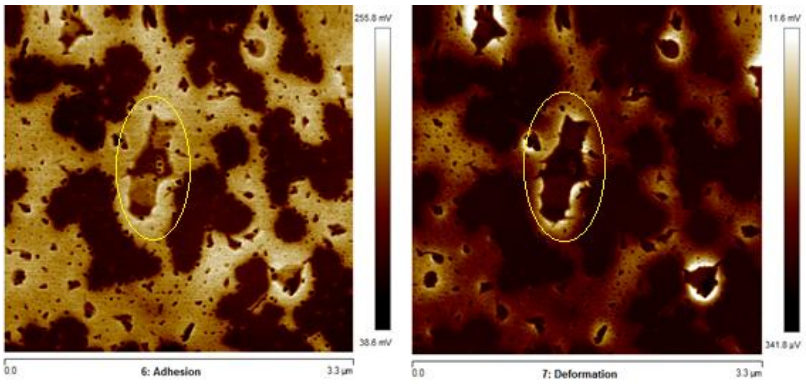

Figure 20: PAni/AGO-0, the adhesion (left) the deformation (right).

TEM analysis of PAni/AGO

The results of the TEM measurements of PAni/AGO-0 on the copper/carbon grid show that there were collections of both sharp edges and also a softer structure, Figure 21. The distinct edges are signs of AGO and the softer and darker part is probably a collection of polyaniline, PAni. What could be seen during the measurement was that the particles which most likely were AGO seemed often to be combined with the PAni.

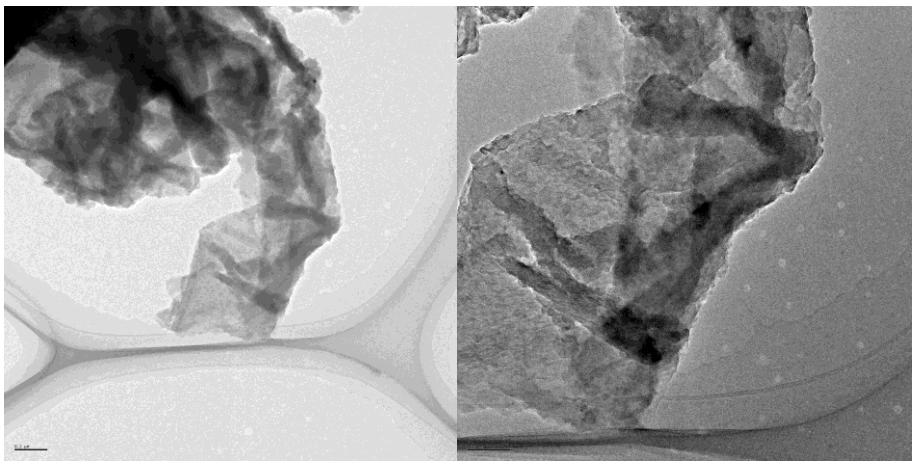

Figure 21: TEM micrographs of PAni AGO. Scale bar is 0.7 µm (left) and 100 nm (right).

4.2.2 Optimization of the PAni/AGO Synthesis

During the synthesis PAni/AGO the cluster formation of AGO and aniline when mixed together in HCl was perceived as a problem for an effective synthesis of polyaniline at the AGO surface. Therefore the process was modified to make the process more effective. For these investigations an AGO load of 1 wt% of the weight of aniline was used.

pH-measurements of the Original Method- PAni/AGO-1

The pH of the synthesis of PAni/AGO was suspected to affect the cluster formation. Therefore a pH electrode was added to the reaction vessel, so the pH could be measured during the reaction. The different reaction steps and pH can be seen in Table 5. The pH measurements shows that the pH increases from 1,5 to a pH of between 4-5. When the initiator is added the pH decreases to around 2.

Table 5: The pH during the PAni/AGO-1

Step no.	Reaction step	pH
1	HCl (0.01 M)	1.5
2	Addition of 1wt% AGO to HCl	1.5
3	Addition of aniline to mixture in step no. 2	4-5
4	Addition of initiator to mixture in step no. 3	~2

When the reaction was finished the product was cleaned as in the original method with distilled water and methanol. 9 mg of the cleaned product was dispersed in 300 µl NMP which gave a PAni/AGO concentration of 30 µg/µl.

Modified Method 1- PAni/AGO-2

The investigated AGO dependence of pH obtained in section 4.1.1 showed that an optimal pH for dispersing AGO is between 4 and 6. Therefore AGO was added to the reaction solution after the aniline. The pH was once again measured and the result can be seen in Table 6. However, the system still formed clusters.

Table 6:The pH changes in PAni/AGO-2 synthesis.

Step no.	**Components in mixture**	**pH**
1	HCl (0.01 M)	1.5
2	Addition of aniline to HCl	5
3	Addition of 1wt% AGO to mixture in step no. 2	4-5
4	Addition of initiator to mixture in step no. 3	~4

Thus, the cluster formation did not seem to have been caused by the pH of the dispersion. Another difference from the original procedure was that the reaction pH did not decrease as for the PAni/AGO-1. The higher pH could have caused that less of the PAni were doped with Cl^- ions. The product was cleaned after the synthesis and 4 mg of cleaned product was dissolved in 133 µl NMP, which gave a PAni/AGO concentration of 30 µg/µl.

Modified Method 2- PAni/AGO-3

Instead of preventing the cluster formation in a chemical way the clusters were dispersed by using ultrasonication. The time needed in the ultra-sonication bath to disperse the cluster was 10 minutes and the AGO/Aniline/HCL aqueous dispersion before and after sonication can be seen in Figure 22.

Figure 22: Before (left) and after (right) ultrasonication of AGO and aniline in HCl.

After the ultra-sonication the reaction vessel was returned to the cooling bath and the initiator was added. The product was cleaned according to the general procedure. 4 mg of the cleaned product was dissolved in 133 µl which resulted in a PAni/AGO concentration of 30 µg/µl.

4.2.3 SEM of PAni/AGO

The SEM micrographs of the PAni/AGO synthesis 0-3 were characterized and compared, see Figures 23-25. Pure PAni can be seen in Figure 26. PAni/AGO-0, with an AGO load of 20wt%, in Figure 23-25a, were analyzed on a steel substrate while the other PAni/AGO-(1-3) were analyzed on SEM aluminum pins.

When the particles in the different mixtures dried on the aluminium SEM pin the flocculation seems to be different. It seems that the modifications of the process had influence on the final character of the samples.

The PAni/AGO-0, Figure 23a has a branched-like structure of the flocs and in between the branches are smaller particles.

PAni/AGO-1 is very similar to the pure PAni structure seen in Figure 23 but the large flocculation's has separated more from each other probably because of the lower concentration in the solvent. The PAni/AGO-1 in Figure 23- 25c, has a large variation of different sizes which can be a result once again of poor homogeneity during the synthesis. The samples in Figure 23-25 a-c are very similar, but differed significantly from the fourth sample, Figure 23-25c that was ultra sonicated during synthesis, PAni/AGO-3.

PAni/AGO-3, in Figure 23-25d shows smaller flocs compared to the other samples. The particles are a little more flakelike as PAni/AGO-0 also is. But for PAni/AGO-0, Figure 23a, the flakes seems to be thinner than in the PAni/AGO-3, Figure 23d.

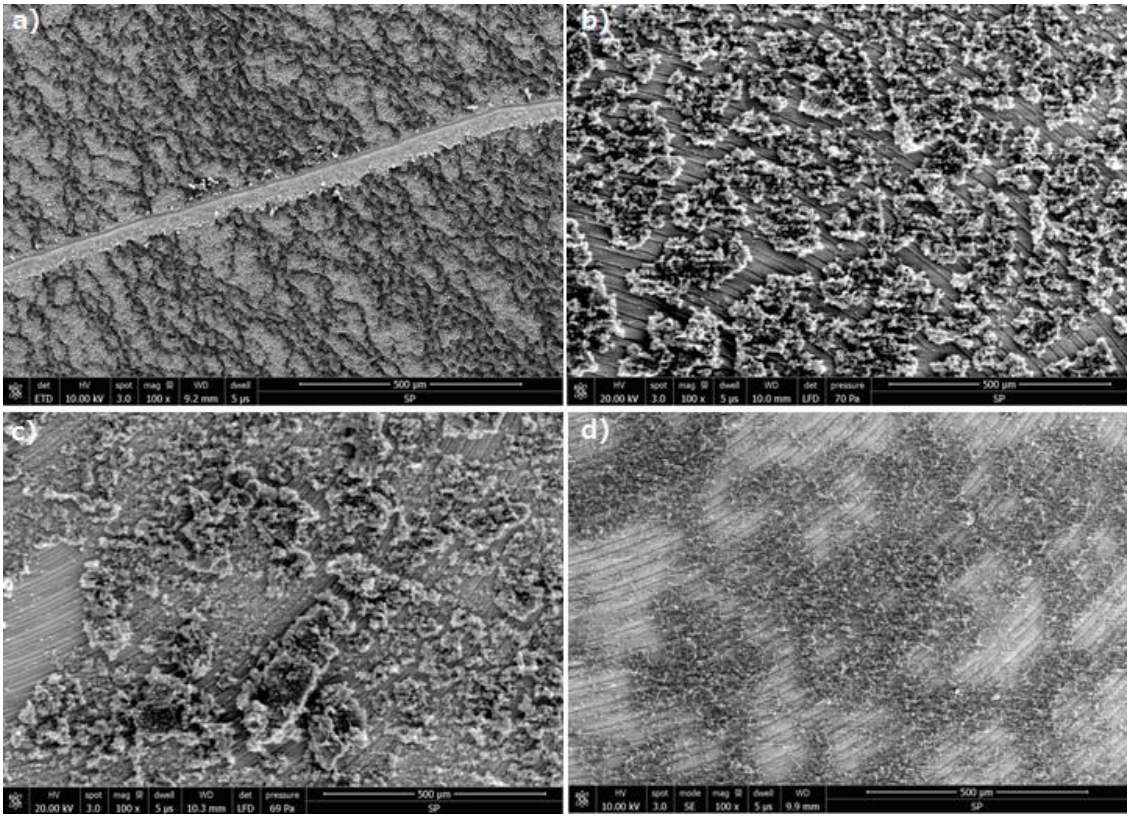

Figure 23: SEM micrographs of a) PAni/AGO-0, b) PAni/AGO-1, c) PAni/AGO-2 and d) PAni/AGO-3. The scale bar is 500 µm.

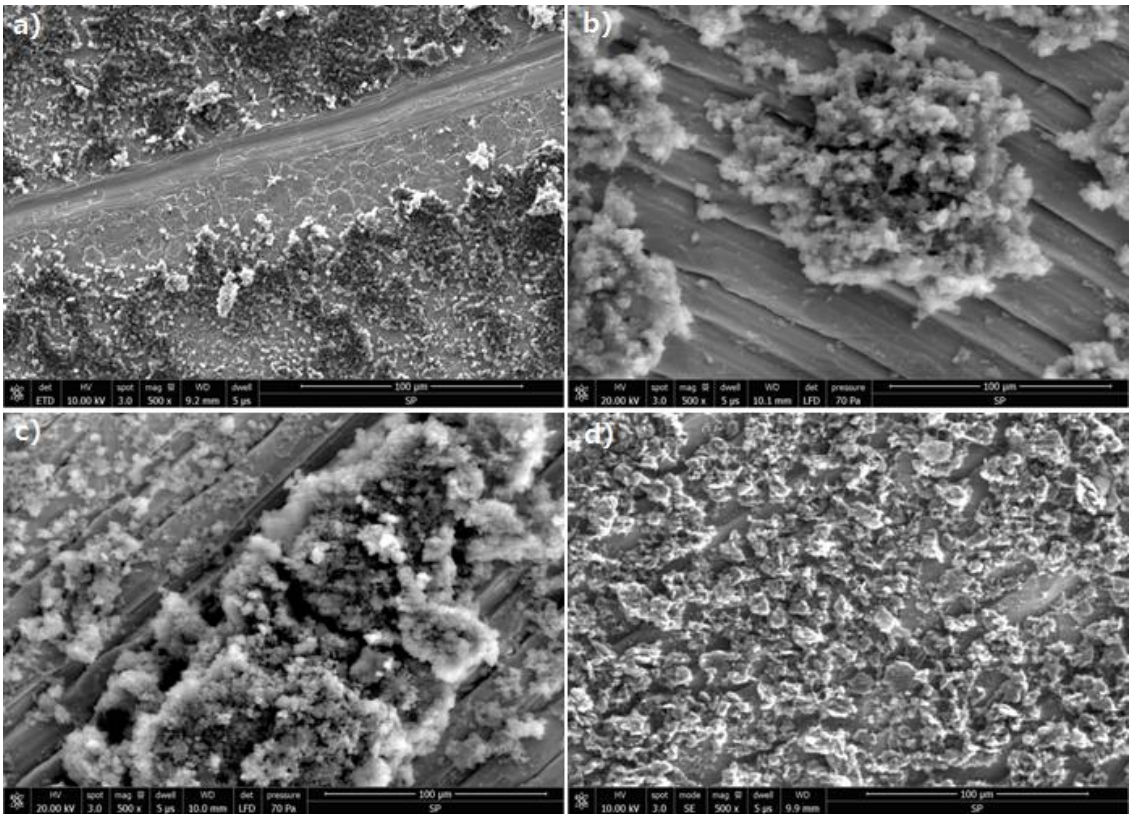

Figure 24: SEM micrographs of a) PAni/AGO-0, b) PAni/AGO-1, c) PAni/AGO-2 and d) PAni/AGO-3. The scale bar is 100 µm.

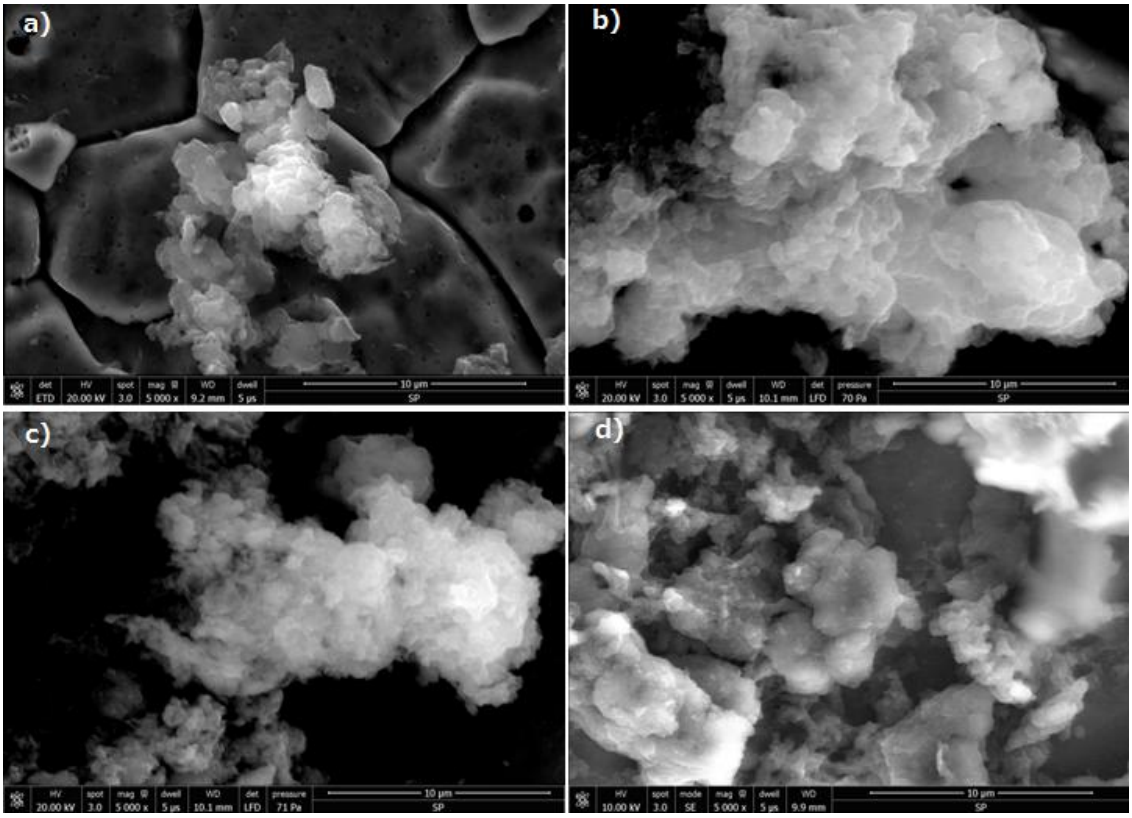

Figure 25: SEM micrographs of a) PAni/AGO-0, b) PAni/AGO-1, c) PAni/AGO-2 and d) PAni/AGO-3. The scale bar is 10 µm.

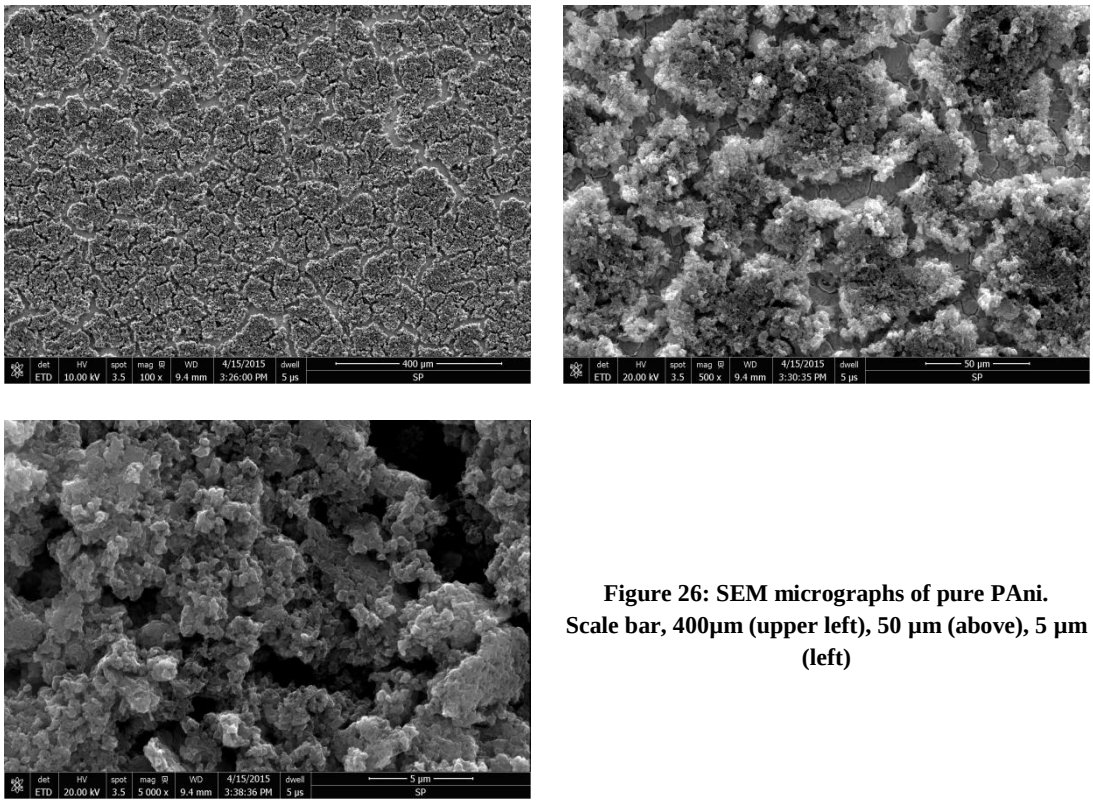

Figure 26: SEM micrographs of pure PAni. Scale bar, 400µm (upper left), 50 µm (above), 5 µm (left)

4.2.4 Raman spectroscopy of PAni/AGO samples

Raman spectra of PAni/AGO and AGO on glass substrate were obtained and analyzed. By comparing the intensity ratios I_D/I_G of PAni/AGO-(0-3) and AGO, some small difference can be seen but the spectra and ratios are generally similar. The intensity ratio of PAni/AGO-1 made by the original method, had an evident higher value than the other ratios demonstrating a higher content of sp^3 hybridized carbons.

By comparing the different synthesis of PAni/AGO-(1-3) it can be seen that PAni/AGO-3 had the highest content of sp^2 hybridized carbons. However, PAni/AGO-3 was not possible to analyze in the same software, Origin, as used for the others and were therefore analyzed in Matlab which creates an uncertainty of the correctness of the numerical result. The numerical peak results can be seen in table 7.

Table 7: The peak intensities of the Raman Spectra of PAni AGO and pure AGO.

Product	I_D (sp^3)	I_G (sp^2)	I_D/I_G	(I_D+I_G)	$I_D/(I_D+I_G)$	$I_G/(I_D+I_G)$
AGO	105.7	102.2	1.03	207.9	0.51	0.49
PAni/AGO-0	166.4	179.1	0.92	345.5	0.48	0.52
PAni/AGO-1	441.5	313.7	1.41	755.2	0.58	0.42
PAni/AGO-2	419.1	358.2	1.17	777.3	0.54	0.46
PAni/AGO-3	1635	1577	1.04	3212	0.51	0.49

The typical peaks for GO is present in all the Raman spectra for PAni/AGO, but as can be seen in the structure of PAni shown in Figure 10 in section 2.6.1, the PAni also contain sp^3 and sp^2 hybridized carbons just like GRMs have. However, pure PAni cannot be analyzed by

Raman spectroscopy due to the darkness of the particles, which mostly gives background scatter. This creates an uncertainty if PAni contribute to the final appearance of the Raman spectra's or if it is only the GRM that contribute to the peaks.

The Raman spectra's are represented in Figures 29-32 in the Appendix.

4.3 Adhesion Aids

Three commercial waterborne binders suitable for corrosion protection of steel were tested and combined with GO_W. The tests were made at ambient temperature and the binders were tested by adding GO_W to investigate the polymer systems response to the GO_W.

The dispersion of GO_W where easily manifested in all the binders disregarding of the GO_W/binder ratio. The binders mixed with GO_W did however change color from white to grey.

Encor 2433 GO_W composite with a GO_W load between 50-90 vol% was tested for adhesion to stainless steel which gave a poor results. Addition of the large amount of GO_W diluted the binder much despite a small load of GO because of the high content of water in GO_W. The high content of water gave the mixtures low viscosity and it became impossible to obtain the wet thickness of 30 µm with the applicator without using a thickener.

Nevertheless the Encor 2433/GO_W coatings were tested for corrosion protection in an application environment which consisted in heating the samples to 70 ^oC in tap water with 3 wt% NaCl. The samples turned darker during the corrosion testing, which were analyzed in Raman spectroscopy as seen in Figure 33 in the appendix.

The sp^3 hybridization of the sample increased after the corrosion testing, see table 8. The change in color of the sample during heating could indicate that the GO_w was reduced during heating to 70 ^oC, since RGO is darker than GO,(described in section 2.2.2 [29]). However, the Raman measurements did not support the hypothesis that reduction of the GO to RGO had occurred. In fact the I_D/I_G ratio increase rather than show the expected decrease, the reason for this is not known.

Table 8: Raman spectroscopy of corrosion tested Encor/GO_W

Product	I_D	I_G	I_D/I_G	I_D+I_G	$I_D/(I_D+I_G)$	$I_G/(I_D+I_G)$
GO_W	56.8	61.4	0.93	118.3	0.48	0.52
Encor GO_W after corrosion test	64.8	56.7	1.14	121.5	0.53	0.47

5. Conclusion

Analysis of GO_W and AGO

The industrially made products GO_W and AGO had almost the same sp^3/sp^2 ratio and both contained single sheet flakes with a sheet thickness between 1-2 nm. The size of GO_W sheets were between 1-7 µm and for AGO they are mostly around or larger than 10 µm. The AGO sheets also tend to fold more than GO_W. When GO and AGO were subjected to ultra-sonication the measured floc/particle size decrease during the first 5 minutes. Sonication for prolonged periods, such as over an hour did not give smaller flocs/particle size, but rather an increase.

Synthesis of PAni/AGO

The pH dependence of AGO was investigated and AGO was most well dispersed at pH 4-6. AGO flocculates more at low pH than at high pH. This indicates that synthesis with AGO should preferably be performed in a pH between 4-6 to achieve the best dispersion of AGO, and the most uniform polymerization on the surface of AGO. However, the pH did not seem to be the reason for the aniline AGO system to flocculate. The flocculated dispersion could be dispersed by ultrasonication.

The cluster formation is probably due to the molecular properties of aniline and AGO, but the exact cause is not known.

Analysis of PAni/AGO

Raman analysis of the different methods showed some differences in the sp^3/sp^2 ratios. The highest amount of sp^3 hybridized carbons were in the original method with 1wt% AGO load. The lowest ratio was observed for the PAni/AGO-0 with an AGO load of 20 wt%.

By comparing the PAni/AGO products from the different synthesis, it was observed that the most flakelike structures of the composite occurred at a high AGO load and when the system was ultra- sonicated. A large load of AGO is thought to be favourable since there seemed to be more thin flakelike structures than in a smaller load which is good for keeping the final coating as thin as possible. The SEM images for the ultrasonicated sample of an AGO load of 1 wt% were also flake like but were thicker than the sample with an AGO load of 20wt%.

The goal of this work was to optimize the PAni/AGO synthesis by having well dispersed AGO at all times. According to the numerical ratio in the Raman spectroscopy and SEM micrographs the ultrasonicated PAni/AGO-3 seem to be the most well dispersed sample, i.e. having the smallest PAni particles.

6. Suggestions for Future Work

The end goal of creating an anti-corrosion coating still needs further development. To investigate the anti-corrosion properties of the nanocomposite synthesized in this work, a coating of the particles need to be made. The PAni/AGO particles do not adhere well to stainless steel which means that adhesion aids are needed for formulation of a coating, The particles made by the different synthesis and GO_W should then be dispersed in the binder, and the resulting coatings investigated for the anti-corrosion properties of the produced particles.

The load of GRMs needs to be optimized. The difference between GO and the RGO should be investigated in the field of corrosion protection.

To improve the binder adhesion to the stainless steel different surface treatments should be investigated.

7. Sources of Uncertainty

The pH measurements of AGO were made on small samples, which could cause a slight pH change when the AGO was added to the solution. The samples were so small that the pH could not be controlled after AGO was added and the particle size could not be measured with the Nanosizer equipment.

There were no confirmation that polyaniline had reacted with AGO, neither if the reaction had succeeded which the kind of substituent group the aniline potentially had reacted with on the AGO sheet.

The PAni/AGO-3 could not be handled by the Origin software for unidentified reasons. The intensity peaks were instead estimated in Matlab2013, with the x-axis as the baseline. This cause an uncertainty of the true values of the Raman spectroscopy results for this sample.

The sources of error of the numerical Raman results were not considered during the investigation of the numerical intensities.

8. Acknowledgements

The work has been preformed within the Strategic Innovation Programme “Grafen” jointly funded by VINNOVA Formas and Energimyndigheten.

Thanks to my two supervisors Dr. Karin Persson at SP and Professor Reine Wallenberg at LTH for support and advising me along this master thesis and refinement of the end report.

At SP would I like to send my gratitude to Dr. Jens Sommertune who provided with polymer expertise and taught me the polyaniline process and made the reference sample of 20 wt% AGO.
Thanks to all of you who helped me in my work:

- Annika Dahlman and Anders Svensk for practical laboratory advises. Mrs Dahlman also assisted with the first SEM micrograph in Figure 13.
- Dr. Viveca Wahlqvist, at SP helped with recording the AFM micrographs seen in Figure 18.
- Rodrigo Robinson helped with SEM micrographs in Figures21-23 and 25.
- Dr. Birgit Brandner for providing and teaching me the basics in Raman Spectroscopy. She provided the Raman spectra in Figures 26-30.
- At LTH Professor Reine Wallenberg also helped me with the TEM micrographs seen in Figure 19.
- At KTH I also want to send my gratitude to Dr. Gunilla Herting and Professor Inger Odenvall Walinder for corrosion expertise.
- At Alfa Laval Dr. Olga Santos for providing the application tests of the adhesion aids.

And lastly thank you all I met during this work, for all interesting discussions and company during the laboratory work. It was a joy to work with you and to have nice people to share this experience with.

All drawings of molecules were made on the https://www.emolecules.com/

References

1. Wang, L., Sundén B., and Manglik R.M., *Plate Heat Exchangers: design, application and performance*. 2007, Great Britain WIT Press. p. 5-6
2. Craig, B.D., Anderson D.S., *Handbook of Corrosion Data*. 2002, USA: ASM Inernational. 8-14.
3. Tjong, S.C., *Polymer Composites with Carbonaceous Nanofillers: Properties and Applications* 2012, Germany: Wiley-VCH Verlag & Co. KGaA. p. 189
4. Fehlner, F.P., Graham M.J., *Thin Oxide Film Formation on Metals*, in *Corrosion Mechanisms in Theory and Practice* M. P., Editor. 2002, Marcel Dekker, Inc. p. 227-230.
5. Davis, J.R., *Corrosion: Understanding the Basics*. 2000, USA: ASM International. p. 1-2, 7-9
6. Bayliss D.A., Deacon D.H., *The corrosion of steel*, in *Steelwork Corrosion Control*. 2002, Spon Press: London. p. 4-6, 8-9.
7. Deflorian, F., *Development of Green Anticorrosion Coatings for Steel Protection based on Environmentally Friendly Nanoparticles and Conducting Polymers*, in *Steel coat*. 2012. www.steelcoatproject.com
8. Wright, G. *Corrosion Protection of Metals*. http://nzic.org.nz/ChemProcesses/metals/8J.pdf the 25th of june 2015
9. Pismenny, A., *Stray current corrosion of carbon steel, electriplated nickel, and electroless, nickel in an alkaline enviroment*, in *Department of Metallurgy and Materials Science*. 2001, University of Toronto. p. 14
10. Ma, F.Y., *Corrosive effects of chlorides on metals*, in *Pitting Corrosion*, N. Bensalah, Editor. 2012: http://www.intechopen.com/books/pittingcorrosion/corrosive-effects-of-chlorides-on-metals.
11. Davis J.R., *Stainless Steels, ASM international Handbook Commitee*. 1999, USA: ASM International. p. 13
12. Zheng, W., Shen B., Zhai W., *Surface Functionalization of Graphene with polymers for Enhanced Properties.* in *New Progress in Graphene Research*, Gong J.R.,2013, InTech
13. Wolf, E.L., *Applications of Graphene An Overview*. 2014, Springer: USA.
14. Chang, C.H., et al., *Novel anticorrosion coatings prepared from polyaniline/graphene composites.* Carbon, 2012. 50(14): p. 5044-5051.
15. Yan Liu, J.Z., Li S., Wang Y., Hana Z., Rena L.; *Fabrication of a superhydrophobic graphene surface with excellent mechanical abrasion and corrosion resistance on a aluminum alloy substrate.* The Royal Society of Chemistry, 2014. 4: p. 45389–45396.
16. Graphenea. *http://www.graphenea.com/products/monolayer-graphene-on-sio2-si-1-cm-x-1-cm*. 4th of May 2015.
17. Paton K.R., e., *Scalable production of large quantities of defect-free few-layer graphene by shear exfoliation in liquids.* Nature Materials, 2014. 13.
18. Zhu, Y., et al., *Graphene and graphene oxide: synthesis, properties, and applications.* Adv Mater, 2010. 22(35): p. 3906-24.
19. Paredes J. I., Villar-Rodil S., Martinez-Alonso A., Tascon J. M. D., *Graphene Oxide Dispersions in Organic Solvents* , Langmuir 2008 , *24* , 10560

20. Hummers W.S., Offeman R.E., *Preparation of Graphitic Oxide*. Journal of the Americal Chemical Soceity 1958. 80 (6), p. 1339–1339
21. Zhao J., Liu L., Li F., *Fabrication and Reduction.*: p. 1-13 in "*Graphene Oxide: Physics & Applications*"; Heidelberg, Springer 2015
22. Konios D., et al., *Dispersion behaviour of graphene oxide and reduced graphene oxide.* J Colloid Interface Sci, 2014. 430: p. 108-12.
23. Rani S., et al., *Characterization and dispersibility of improved thermally stable amide functionalized graphene oxide.* Materials Research Bulletin, 2014. 60: p. 143-149.
24. Shih C.J., et al., *Understanding the pH-dependent behavior of graphene oxide aqueous solutions: a comparative experimental and molecular dynamics simulation study.* Langmuir, 2012. 28(1): p. 235-41.
25. http://www.graphenea.com/products/reduced-graphene-oxide-1-gram, *Reduced Graphene oxide*, Graphenea, Editor. 2015 (1th of June).
26. Wang L., et al., *Graphene-based polyaniline nanocomposites: preparation, properties and applications.* J. Mater. Chem. A, 2014. 2(13): p. 4491-4509.
27. Zhu C., Guo S., Fang Y., Dong S., *Reducing Sugar New Functional molecules for the green synthesis of graphene nanosheets.* American Chemical Society, 2010. VOL. 4(NO. 4): p. 2429–2437.
28. Jaemyung Kim, F.K.a.J.H., *Seeing graphene-based sheets.* Materials Today 2010. 13.
29. Shang Y., D.Z., Yanyun Liu and C. Guo, *Preliminary comparison of different reduction methodes of graphene oxide.* Bull. Mater. Sci.,, 2014. 38(1).
30. Su Y., et al., *Impermeable barrier films and protective coatings based on reduced graphene oxide.* Nat Commun, 2014. 5: p. 4843.
31. Myers, R., *The Basics of Chemistry*. 2003, Greenwood Press: USA.
32. Ma, W.-S., J. Li, and X.-S. Zhao, *Improving the thermal and mechanical properties of silicone polymer by incorporating functionalized graphene oxide.* Journal of Materials Science, 2013. 48(15): p. 5287-5294.
33. Minko, S., *Grafting on Solid Surfaces: "Grafting to" and "Grafting from" Methods*, in *Polymer Surfaces and Interfaces*, M. Stamm, Editor. 2008, Springer.
34. Bhattacharya, A. and P. Ray, *Basric Features and Techniqes*. Polymer Grafting and Crosslinking. 2009: Johan Wiley Sons, inc. .
35. Wang, M., et al., *Enhanced interfacial thermal transport across graphene–polymer interfaces by grafting polymer chains.* Carbon, 2015. 85: p. 414-421.
36. Tritt T., *Thermal Conductivity: Theory, Properties, and Applications*. Kluwer Academic/Plenum Publisher. 2004 New York p. 9
37. Lienhard IV J.H., Lienhard V J.H., *A Heat Transfer Textbook*. Fourth ed. 2012, USA: Phlogston Press.
38. Serov, A.Y., Z.-Y. Ong, and E. Pop, *Effect of grain boundaries on thermal transport in graphene.* Applied Physics Letters, 2013. 102(3): p. 033104.
39. Yavari, F., et al., *Enhanced Thermal Conductivity in a Nanostructured Phase Change Composite due to Low Concentration Graphene Additives.* The Journal of Physical Chemistry C, 2011. 115(17): p. 8753-8758.

40. Tong, X.C., *Thermally Conductive Polymer Matrix Composites*, in *Advanced Materials for Thermal Management of Electronic Packaging*. 2011, Springer ScienceþBusiness Media.
41. Cowie J.M.G, Arrighi V., *Polymers: Chemistry and Physics of Modern Matierials*. Third Edition ed. 2008, USA: CRC Press.
42. Schwamb, T., et al., *An electrical method for the measurement of the thermal and electrical conductivity of reduced graphene oxide nanostructures.* Nanotechnology, 2009. **20**(40): p. 405704.
43. Mu, X., et al., *Thermal transport in graphene oxide--from ballistic extreme to amorphous limit.* Sci Rep, 2014. **4**: p. 3909.
44. *ASM Ready Reference: Thermal properties of metals*, F. Cverna, Editor. 2002, ASM International: USA.
45. Nath, C., et al., *Heat conduction in conducting polyaniline nanofibers.* Applied Physics Letters, 2013. **103**(12): p. 121905.
46. *Thermal Properties of Plastic Materials*, Profesional Plastics, Datasheet. http://www.professionalplastics.com/professionalplastics/ThermalPropertiesofPlastic Materials.pdf
5th of May
47. Pashley R.M., Karaman M.E., *Applied colloid and surface chemistry* 2004, England: John Wiely and sons, Ltd.
48. Hunter R.J., *Zeta Potential in Colloid Science: Principles and Applications,*1988, Great Britain, the Alden Press, Osney Mead, Oxford
49. Everett, D.H., *Basic Principles of Colloid Science*. 1988, Kent: Whitstable Litho Ltd. p. 90
50. Mittal V., *Polymer-Graphene Nanocomposites*. 2012, Publisher RSC, United Kingdom
51. Aldrich, S., h*ttp://www.sigmaaldrich.com/catalog/product/aldrich/763705?lang=en&region=SE*. 5th of May 2015.
52. Bracamonte, M.V., et al., *On the Nature of Defects in Liquid-Phase Exfoliated Graphene.* The Journal of Physical Chemistry C, 2014. **118**(28): p. 15455-15459.
53. Yeole, N., S.N. Kutcherlapati, and T. Jana, *Polystyrene-graphene oxide (GO) nanocomposite synthesized by interfacial interactions between RAFT modified GO and core-shell polymeric nanoparticles.* J Colloid Interface Sci, 2015. **443**: p. 137-42.
54. Kotsilkova, R., *Rheological approach to nanocomposite design*, in *Thermoset Nanocomposites for Engineering Applications*, R. Kotsilkova, Editor. 2007, Smithers Rapra Technology Limited: UK.
55. Lin, S.J., et al., *Synthesis of high-performance polyaniline/graphene oxide nanocomposites.* High Performance Polymers, 2014. **26**(7): p. 790-797.
56. Konkena, B. and S. Vasudevan, *Understanding Aqueous Dispersibility of Graphene Oxide and Reduced Graphene Oxide through pKaMeasurements.* The Journal of Physical Chemistry Letters, 2012. **3**(7): p. 867-872.

57. Parmar, M., C. Balamurugan, and D.W. Lee, *PANI and graphene/PANI nanocomposite films--comparative toluene gas sensing behavior.* Sensors (Basel), 2013. **13**(12): p. 16611-24.
58. Laslau, C., Z. Zujovic, and J. Travas-Sejdic, *Theories of polyaniline nanostructure self-assembly: Towards an expanded, comprehensive Multi-Layer Theory (MLT).* Progress in Polymer Science, 2010. 35(12): p. 1403-1419.
59. Stankiewicz, A., I. Szczygieł, and B. Szczygieł, *Self-healing coatings in anti-corrosion applications.* Journal of Materials Science, 2013. 48(23): p. 8041-8051.
60. Kaner, J.H.a.R.B., *Polyaniline Nanofibers: Syntheses, Properties and Applications*, in *Conjugated Polymers Theory, Synthesis, Properties and Characterization*, A.S.a.J.R. Reynolds, Editor. 2007, CRC Press Taylor and Francis Group: USA.
61. Guetta, D. *Acidity Basicity kPa*. 2006. http://www.columbia.edu/~crg2133/Files/CambridgeIA/Chemistry/AcidityBasicitykPa.pdf 19th May 2015
62. *http://research.cm.utexas.edu/nbauld/CHAPTER%2021.htm*. 19th of May 2015
63. Chang, K.-C., et al., *Room-temperature cured hydrophobic epoxy/graphene composites as corrosion inhibitor for cold-rolled steel.* Carbon, 2014. **66**: p. 144-153.
64. Yu, Y.-H., et al., *High-performance polystyrene/graphene-based nanocomposites with excellent anti-corrosion properties.* Polym. Chem., 2014. **5**(2): p. 535-550.
65. John R. Ferraro, K.N.a.C.W.B., *Introductory Raman Spectroscopy*. Second ed. 2003: Academic Press.
66. Gayathri, S., et al., *Synthesis of few layer graphene by direct exfoliation of graphite and a Raman spectroscopic study.* AIP Advances, 2014. **4**(2): p. 027116.
67. In, J.Y.a.I., *Enhanced solvent exfoliation of graphene dispersion in the presence of polymer additive.* Chemical letter, 2011(40): p. 567-569.
68. Yang, H., et al., *Rapid and non-destructive identification of graphene oxide thickness using white light contrast spectroscopy.* Carbon, 2013. **52**: p. 528-534.
69. Moore, L.E.S.a.E.A., *Solid state Chemistry an Introduction* Fourth ed. 2012, London: CRC Press Taylor & FRancis Group
70. http://www.sigmaaldrich.com/catalog/product/aldrich/777013?lang=en&region=SE the 25th of June 2015

Appendix

Raman Spectra

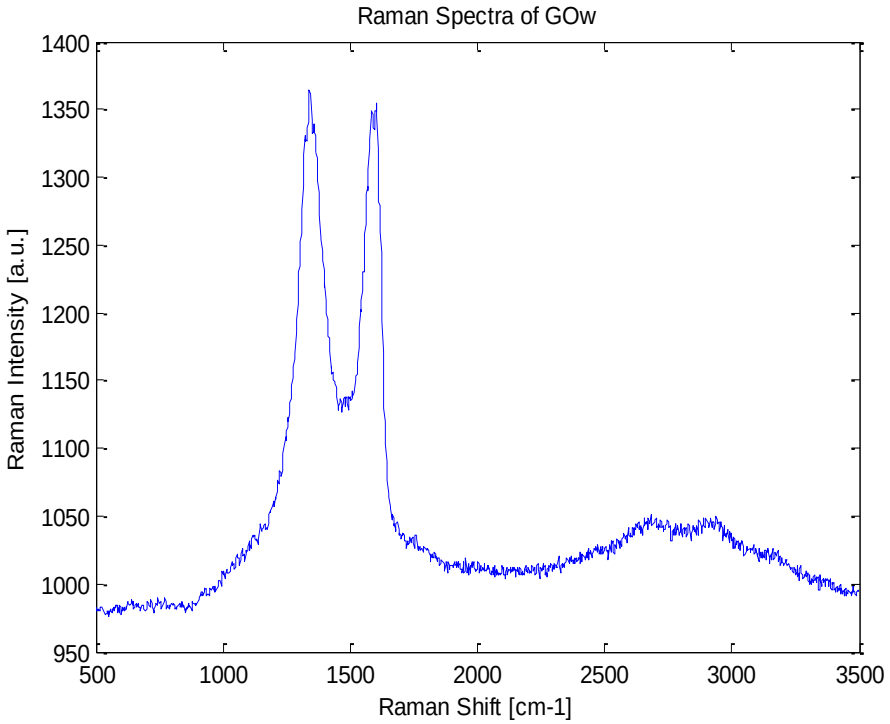

Figure 27: Raman spectra of GO_w

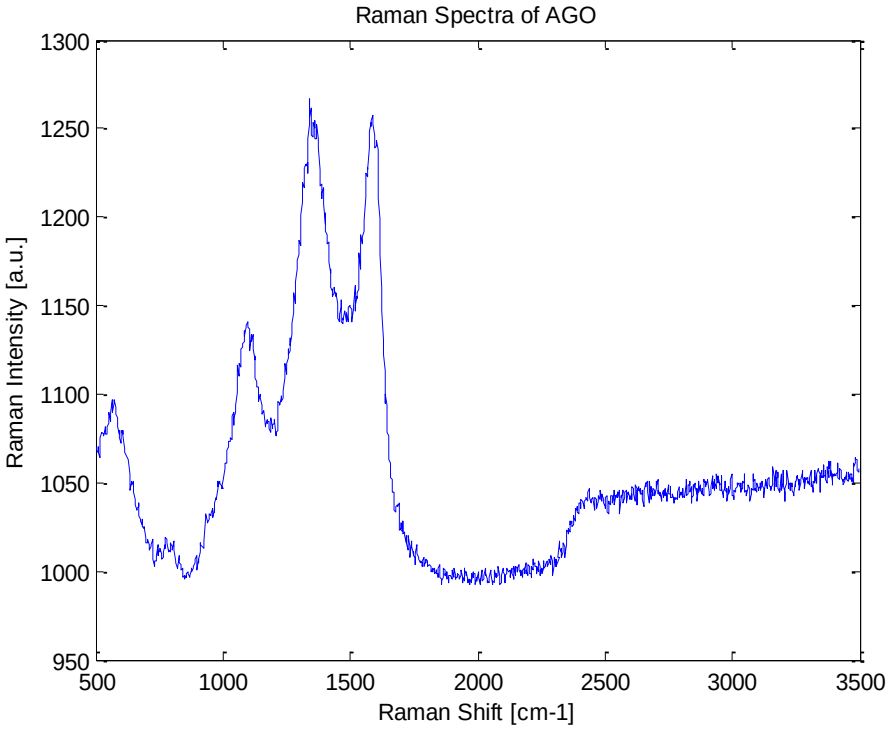

Figure 28: Raman spectra of AGO

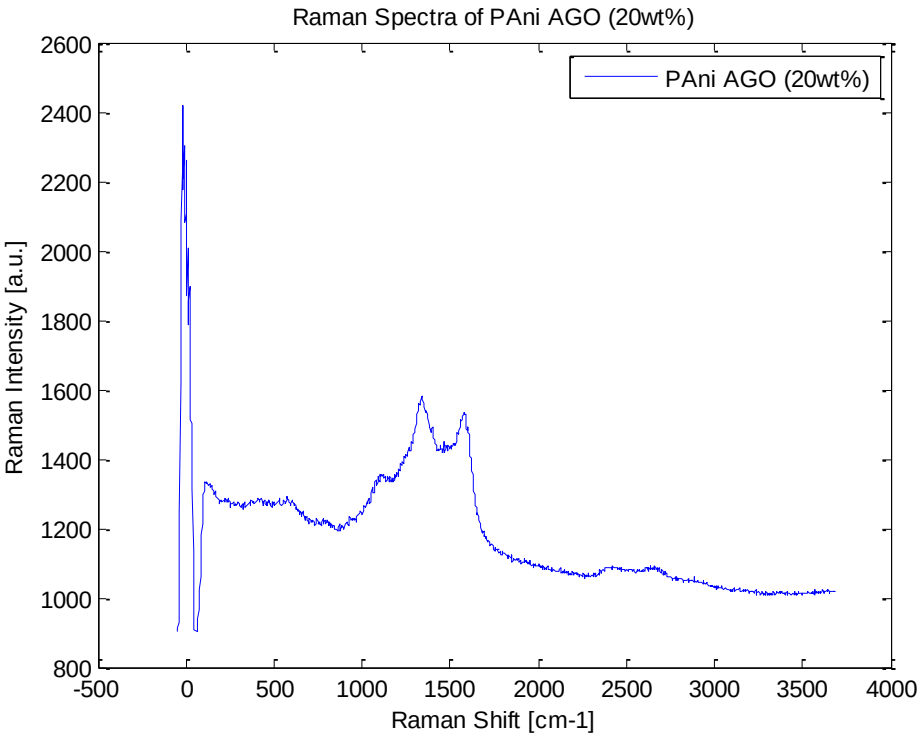

Figure 29: Full Raman spectra of PAni/AGO-0

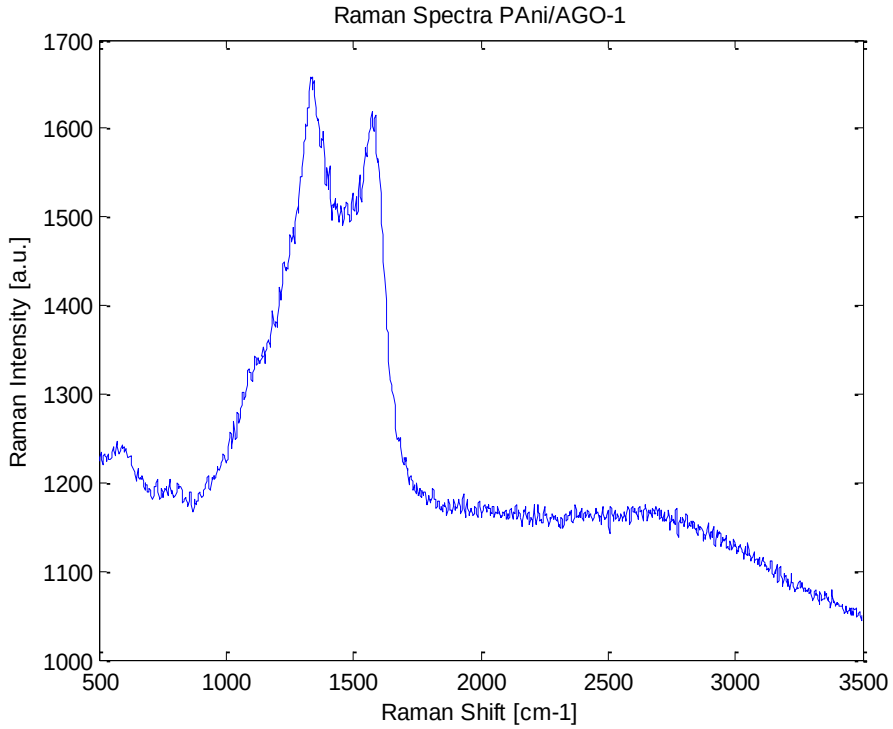

Figure 30: Raman Spectra of PAni/AGO-1

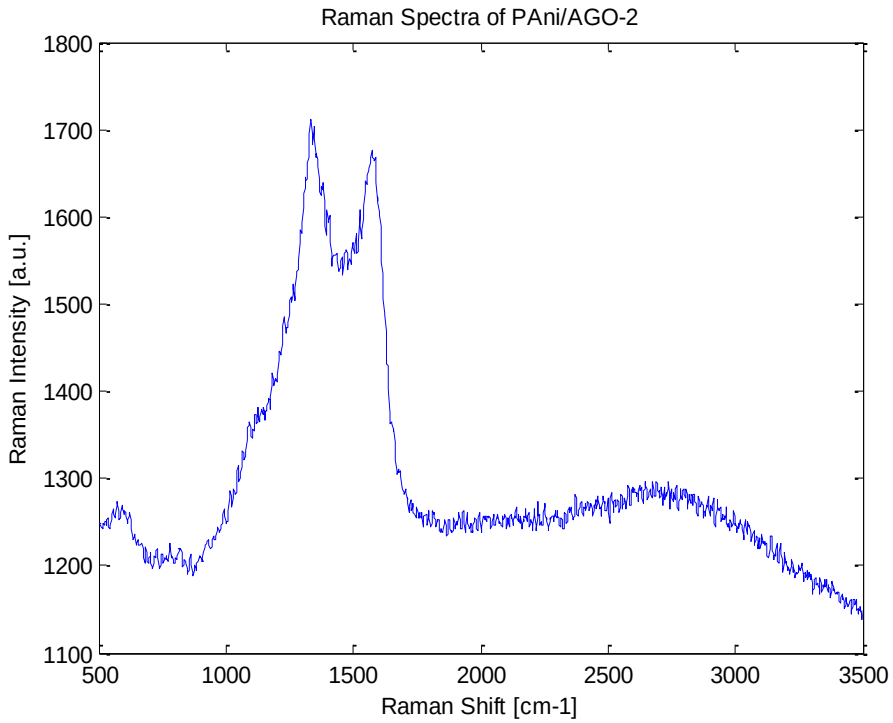

Figure 31: Raman spectra of PAni/AGO-2

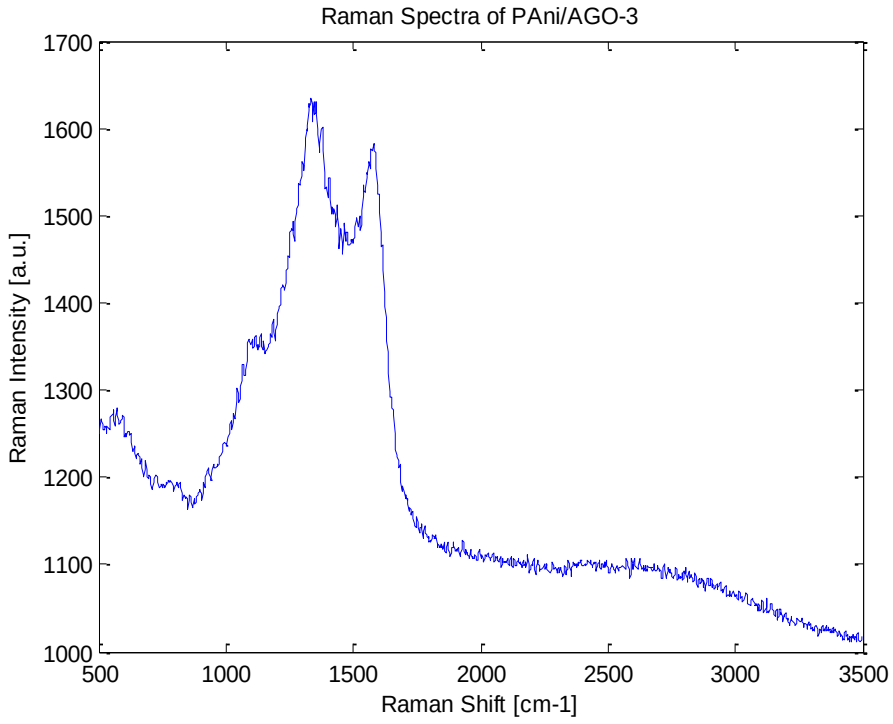

Figure 32: Raman spectra of PAni/AGO-3

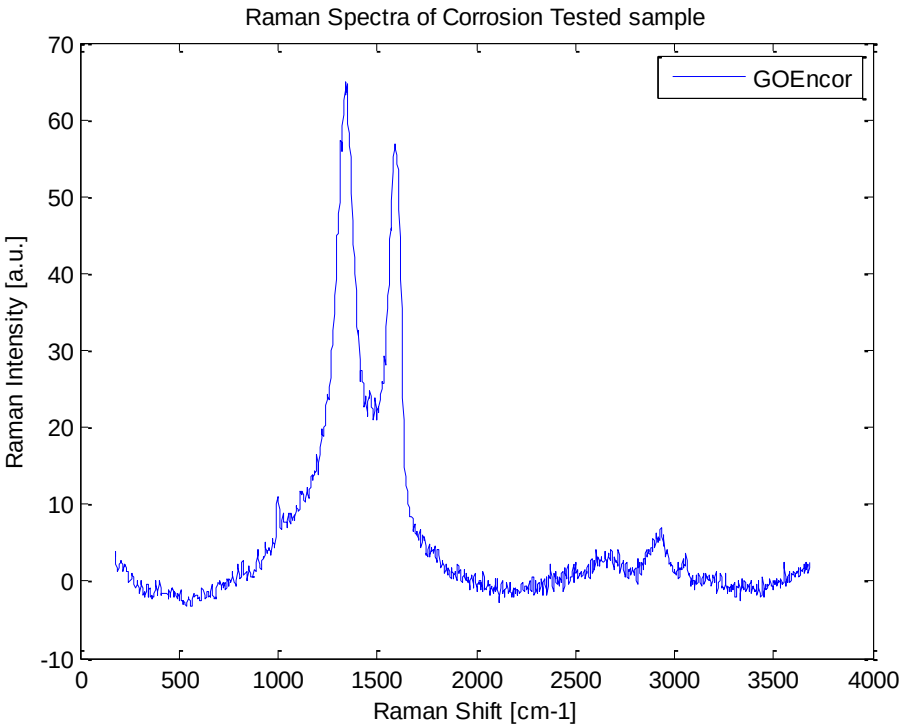

Figure 33: Full Raman spectra of 50vol% GO Encor which were corrosion tested

Additional Experiment

Six samples GO_W was casted on glass and were dried in the fume hood for one day.
The samples were then placed in beakers containing MilliQ water, tap water with 3 wt% NaCl and the third containing ASTM lake water, two of each. Three beakers, one with each medium, were placed in room temperature and the other three were heated to 70 ^oC for two hours.

Results

The samples placed in Milliq water fell apart in small pieces if the beakers were shaken.
The samples containing salts in room temperature were not affected. The samples containing salts and were heated dismantled from the glass substrate and floated as a coherent flake.
When this experiment were performed with AGO, the same phenomena occurred but took several days instead, of two hours.

Conclusion

The coherent flakes only appear in solutions containing chloride ions. It appeared for both GO_W and AGO which may indicate that chloride ions in combination with increased temperature increase the coherence in GRMs. It is possible that this occurs at lower temperatures as well but here it was only seen at temperatures around 70 ^oC. The longer time for AGO to obtain the same phenomena could have been caused by stronger bonds between the ammonia groups on the graphene sheet and the glass substrate.

Washing procedure of steel substrate made by SP

Chemical name	**Formula**	**Supplier**	**CAS**
Acetone	$CH_3(CO)CH_3$	Solveco	67-64-1
Isopropanol	C_3H_7OH	Solveco	67-63-0
Nitric acid	HNO_3	Fisher lab	7697-37-2
MilliQ water	H_2O	-	-

Method

The steel substrate was first cleaned by washing the pieces in acetone and isopropanol for 3-5 seconds each. The pieces were then placed in a beaker with acetone in an ultrasonication bath for 3 minutes and thereafter the same procedure was performed in isopropanol.
After the sonication procedure the steel samples were placed in an acid bath with 16 wt% HNO_3 for 40 minutes. The samples were thereafter washed three times with milliQ water and dried under a flow of nitrogen and placed on filter paper covered with a polymer film to avoid contact between the substrates.